

ABSTRACT

FREY, MARGARET LOUISE. Regional and Interannual Comparisons of Marine Stratocumulus Precipitation. (Under the direction of Sandra E. Yuter).

Marine stratocumulus clouds are a ubiquitous feature of subtropical marine boundary layers. These clouds form in the atmospheric boundary layer above oceanic upwelling zones off the western coasts of continents. These low-lying, high albedo clouds are a key component in the global radiation budget but are poorly parameterized in global climate models.

Precipitation, in the form of drizzle, is known to incite changes in cloud fraction and hence alter the radiative properties of a particular cloud sheet. This work is the first to combine an examination of marine stratocumulus diurnal and interannual variability of drizzle occurrence with a comparison among the three main marine stratocumulus geographic regions – the Southeast Pacific (SEP), the Northeast Pacific (NEP), and the Southeast Atlantic (SEA). Passive microwave measurements, from the Advanced Microwave Scanning Radiometer-EOS (AMSR-E) 89 GHz channel, are used in tandem with sea surface temperature and integrated water vapor data as input to an empirical algorithm that yields a binary heavy drizzle (liquid water path $> 200 \text{ g m}^2$) detection product. The entire period of AMSR-E availability (2002-2011) is exploited to analyze precipitation frequency and interannual variability. The SEP is the only region where seasonal drizzle frequency reaches 30% during the season with lower-tropospheric static stability maxima (Sept., Oct., Nov.). All regions exhibit interannual variability and a strong diurnal cycle. Seasonal sea surface temperature and cloud droplet number concentrations are compared to drizzle occurrence frequency in each region of interest. The environmental controls on marine stratocumulus drizzle are complex and numerous; high cloud droplet number concentrations ($> 130 \text{ cm}^{-3}$) near the western coasts of continents limit cloud droplet growth and reduce the probability of heavy drizzle. Further from the coast, boundary layer depth increases as sea surface temperatures increase and the probability of heavy drizzle increases. During the strong negative (cool) La Nina of 2010 nighttime precipitation is maximized in the SEP and NEP.

© Copyright 2013 by Margaret Louise Frey

All Rights Reserved

Regional and Interannual Comparisons of Marine Stratocumulus Precipitation

by
Margaret Louise Frey

A thesis submitted to the Graduate Faculty of
North Carolina State University
in partial fulfillment of the
requirements for the degree of
Master of Science

Marine, Earth and Atmospheric Sciences

Raleigh, North Carolina

2013

APPROVED BY:

Sandra Yuter
Committee Chair

Walter Robinson

Peter Thorne

BIOGRAPHY

I grew up rural in Michigan before attending high school in a suburb of Washington, D.C. An avid skier, it was a childhood curiosity with snowfall forecasts that sparked my interest in this field. I attended the University of Oklahoma and graduated in 2006 with a B.S. in Meteorology and minors in Mathematics and Spanish. Although I now find myself engaged in research that remains strictly liquid-phase, my enthusiasm for meteorology has not waned. In the future I plan on working for the National Park Service as a field technician and will ultimately pursue a PhD in order to become a faculty member at a four-year university.

ACKNOWLEDGMENTS

I cannot express enough gratitude to my parents, Chris and Annette Frey. I have their unyielding support in whatever ventures I pursue and I expect them to visit me at all of my future destinations.

I was lucky enough to become a member of the Cloud and Precipitation Processes and Patterns Group at NCSU in Spring 2011. It is because of both former and current group members (all three named Matt, Andrew, Casey, Nate, Tai, Cam, Nicole, Jeff, Lani, Dianna, and Jennifer) that I have managed to complete my graduate studies relatively unscathed.

And who could forget our imperious leader – Dr. Sandra Yuter. Her enthusiasm, diligence, prowess, and patience create a collaborative space for intellectual growth. If more graduate students were exposed to such mentorship, I have no doubt the critical thinking and interpersonal skills of the student population would increase twofold.

And to my friends – thank you for your humor and all of the subsequent laughter.

TABLE OF CONTENTS

LIST OF TABLES	vi
LIST OF FIGURES	vii
Chapter 1 Introduction	1
Chapter 2 Data and Methods	6
2.1 Areas of Interest.....	6
2.2 Satellite-Derived Precipitation Detection.....	6
2.3 89 GHz Algorithm Over Terrestrial Surfaces.....	8
2.4 Ancillary Satellite-Derived Cloud Characteristics.....	9
2.5 Data Processing Method.....	9
2.6 Ice-Phase Cloud Mask.....	10
Chapter 3 Regional Precipitation Frequency Distributions	15
3.1 Introduction.....	15
3.2 Southeast Pacific.....	16
3.3 Northeast Pacific.....	17
3.4 Southeast Atlantic.....	18
3.5 Regional Contrasts.....	20
Chapter 4 Interannual Precipitation Trends	26
Chapter 5 Comparison of Regional Environmental Parameters	31
Chapter 6 Conclusions	35
6.1 Discussion.....	35
6.2 Future Work.....	36

References	37
APPENDIX	43

LIST OF TABLES

Table A1.1 Dataset overview.....	44
Table A1.2 Precipitation frequencies (SEP, SON, nighttime).....	45
Table A1.3 Precipitation frequencies (SEP, SON, daytime).....	46
Table A1.4 Precipitation frequencies (NEP, JJA, nighttime).....	47
Table A1.5 Precipitation frequencies (NEP, JJA, daytime).....	48
Table A1.6 Precipitation frequencies (SEA, SON, nighttime).....	49
Table A1.7 Precipitation frequencies (SEA, SON, daytime).....	50

LIST OF FIGURES

Figure 2.1 Annual stratocumulus cloud cover with areas of interest outlined.....	12
Figure 2.2 C-band radar reflectivities from VOCALS field campaign.....	13
Figure 2.3 Comparison of AMSR-E and MODIS LWP with binary drizzle product.....	14
Figure 3.1 Drizzle frequency in the Southeast Pacific.....	21
Figure 3.2 Drizzle frequency in the Northeast Pacific.....	22
Figure 3.3 Drizzle frequency in the Southeast Atlantic.....	23
Figure 3.4 Cloud top temperature distributions by region, time, and season.....	24
Figure 3.5 Mean scene precipitation distributions by region, time, and season.....	25
Figure 4.1 Precipitation area frequencies by season, region, and year.....	28
Figure 4.2 Nighttime seasonal drizzle frequency maxima and minima.....	29
Figure 4.3 Daytime seasonal drizzle frequency maxima and minima.....	30
Figure 5.1 Seasonal drizzle frequency, cloud droplet number concentration, and sea surface temperature fields for 2003 and 2004.....	33
Figure 5.2 Drizzle occurrence compared to sea surface temperature and cloud droplet number concentrations.....	34
Figure A1.1 Ice-phase cloud frequency in the Southeast Pacific.....	51
Figure A1.2 Ice-phase cloud frequency in the Northeast Pacific.....	52
Figure A1.3 Ice-phase cloud frequency in the Southeast Atlantic.....	53
Figure A1.4 Nighttime drizzle frequency by season and year (2002-2007).....	54
Figure A1.5 Nighttime drizzle frequency by season and year (2007-2011).....	55
Figure A1.6 Daytime drizzle frequency by season and year (2002-2007).....	56
Figure A1.7 Daytime drizzle frequency by season and year (2007-2011).....	57

Chapter 1 – Introduction

Marine stratocumulus clouds cover expansive areas of the subtropical ocean off the west coasts of California, Peru, and Namibia and span a geographic area of $8 * 10^6$ km² during peak seasonality, an area roughly twice the size of Alaska (Klein and Hartmann 1993; Hahn and Warren 2007). Oceanic upwelling and large-scale subsidence driven by global circulations act to create a cool, shallow boundary layer – an ideal thermodynamic environment for the development and maintenance of marine stratocumulus clouds. Marine stratocumulus clouds are a source of net cooling in the global radiation budget. Marine stratocumulus clouds are of particular interest to the climate modeling community as a 4% increase in coverage would offset a global temperature increase of 2-3 K (Randall et al. 1984). Future areal trends of these expansive, areal clouds are of key concern – an increase in coverage could offset warming but a decrease in cloud coverage could enhance current temperature trends (Clement et al. 2009; Eastman et al. 2011).

Overall, most global climate models poorly represent stratocumulus cloud properties relevant to albedo and radiation (Comstock et al. 2005; Medeiros et al. 2012). More confounding to global climate models is the parameterization of the stratocumulus precipitation process (Pawlowska and Brenguier 2003; Wang and Feingold 2009). Cloud resolving models convert cloud liquid water to precipitation-sized particles too rapidly and thus misrepresent the observed frequency of precipitation (Suzuki et al. 2011; Berner et al. 2011).

The radiative characteristics of marine stratocumulus clouds are closely tied to cloud fraction. Drizzle, the type of precipitation inherent to these low-lying clouds, is associated with changes in scene cloud fraction (Stevens et al. 2005; Comstock et al. 2007; Stevens et al. 2007). Drizzle is currently understood to be a necessary but not sufficient condition in the closed- to open-cellular transitions that result in decreased cloud fraction (Wood et al. 2011). Drizzle is also associated with enhanced mesoscale variability. Light drizzle that evaporates before reaching the surface increases boundary layer stratification and aids in cumulus formation below the stratocumulus deck (Feingold et al. 1996; Feingold et al., 2010); heavy drizzle further promotes boundary layer decoupling and is known to incite cloud breakup (Comstock et al. 2007; Burleyson et al. 2013). The removal of sub-cloud moisture by drizzle affects the thickness of the saturated layer, thus promoting cloud thinning and dissipation (Ackerman et al. 1993). Furthermore, drizzle is a key link between macrophysical and microphysical cloud processes. Drizzle can initiate the formation of large-scale cold pools (Terai 2011) and alter aerosol concentration due to sedimentation (Wood 2012).

The main focus of this study is to elucidate heavy drizzle frequency across the three primary subtropical marine stratocumulus regions. For this purpose, heavy drizzle is defined as a liquid water path in exceedence of $200 \text{ g}\cdot\text{m}^2$, this threshold value is further discussed in Chapter 2. An algorithm based on 89 GHz brightness temperatures from the Advanced Microwave Scanning Radiation –EOS (AMSR-E) instrument and sea surface temperatures from the Moderate Resolution Imaging Spectroradiometer (MODIS) are used to create a precipitation frequency product at $4 \text{ km} \times 6 \text{ km}$ resolution. This resolution is currently the

finest available for nighttime scenes. The 89 GHz algorithm has been evaluated against satellite-based liquid water path measurements and ship-based radar observations, the full methodology is discussed at length in Miller and Yuter (2013).

This study utilizes the entire AMSR-E dataset, 108 months of twice daily observations, to make conclusions regarding the seasonality of observed precipitation and changes in diurnal and seasonal amplitude in each stratocumulus region. The spatial resolution of the 89 GHz algorithm is high enough to resolve individual drizzling cells, known to have a 4-6 km horizontal length scale (Atkinson and Zhang 1996). The data are available twice a day at ~1:30 a.m. and ~1:30 p.m. (King et al. 1997) which is near the drizzle frequency maxima (3 a.m.) and minima (3 p.m.) (Burleyson et al. 2013). The dataset spans nine years, 2002-2011, allowing for a complete analysis of seasonal and interannual precipitation variability.

Previous work that has attempted to characterize the macrophysical and microphysical variability associated with stratocumulus precipitation has focused on daytime retrievals of atmospheric parameters (Kubar et al. 2009) and has used a year or less of measurements (Leon et al. 2008). Any study that does not include nighttime retrievals does not account for the mode of precipitation frequency. It is well understood that marine stratocumulus cloud fraction exhibits seasonal variability (Klein and Hartmann 1993; Ghate et al. 2009) with cloud coverage peaking during the season of maximum lower-tropospheric stability. Drizzle is most prevalent at night (Burleyson et al. 2013), but the amplitude between daytime and nighttime observations has not been compared across the three regions of interest.

The primary stratocumulus regions of interest are the cloud decks that occur off the coasts of California/Baja California, Peru and Namibia. While extensive field campaigns have been dedicated to the study of the Californian (Lenschow et al. 1988; Stevens et al. 2003) and Peruvian cloud decks (Bretherton et al. 2004; Wood et al. 2011), the Namibian stratocumulus regime has not yet been observed in a field campaign. Though the Australian, Azorian, and Canarian stratocumulus regions are also considered to be important regimes because of high annual low-cloud coverage (Hahn and Warren 2007; Leon et al. 2008), analyses of precipitation frequency in these regions is beyond the scope of this study as the synoptic forcings are more nuanced than the three primary regions highlighted in this study. Mid-latitude cyclonic systems and associated cold fronts, as opposed to semi-permanent high pressure circulations, may be the dominant large-scale mechanism for the Australian, Azorian, and Canarian stratocumulus cloud decks. The three regions of focus in this study have a markedly low air-sea temperature difference of 1-2° (Comstock et al. 2005) and higher static stability maxima (Klein and Hartmann 1993).

In the three regions of interest it is hypothesized that there will be little interannual variability and similar spatial heterogeneity of precipitation across the three regions. A marked diurnal cycle of precipitation frequency is expected among each region, with most drizzle expected to occur at night when cloud fraction is more variable (Comstock et al. 2004; Leon et al. 2008; Burleyson et al. 2013). In the Southeast Pacific it has been suggested that mesoscale and sub-mesoscale mechanisms play a crucial role in modulating cellular convection and hence precipitation (Wood and Hartmann 2006). Other studies confirm that neither large-

scale forcings nor topography play an important role in modulating cellularity in the Southeast Pacific (Richter and Mechoso 2006) and Namibian region (Richter and Mechoso 2004). Changes in boundary layer stability due to sea surface temperature variation (Mitchell and Wallace 1992) may prove relevant when comparing seasonal precipitation trends across the three regions.

The full scope of this work is presented the following sections: Chapter 2 Data and Methods, Chapter 3 Regional Precipitation Frequency Distributions, Chapter 4 Interannual Precipitation Trends, Chapter 5 Comparison of Regional Environmental Parameters and Chapter 6 Conclusions.

Chapter 2 – Data and Methods

2.1 Areas of Interest

The areas of interest in this study contain the marine stratocumulus cloud decks in the Northeast Pacific off the coast of California/Baja California, in the Southeast Atlantic off the coast of Namibia, and in the Southeast Pacific off the coast of Peru; throughout this study the regions are referred to as NEP, SEA, and SEP, respectively. The geographic bounds for each region are determined based on an evaluation of low stratiform coverage from the International Comprehensive Ocean-Atmospheric Data Set (Klein and Hartmann 1993; Woodruff et al. 2011), stratiform precipitation maxima (Leon et al. 2008) and annual stratocumulus maxima as determined from the Climatic Atlas of Clouds Over Land and Ocean (Figure 2.1) (Hahn and Warren 2007). The bounds used in this analysis are 35° by 35° and are therefore large enough to detect the entire spatial extent of the marine stratiform precipitation zones. Using one year of CloudSat data, Leon et al. 2008 showed localized regions of high precipitation frequency within the areas of interest which this study seeks to verify.

2.2 Satellite-Derived Precipitation Detection

The methodology used for the analysis of each overpass time is discussed at length in Miller and Yuter (2013) and is briefly summarized here. Although usually employed as an ice scattering channel, passive microwave retrievals at 89 GHz are also sensitive to emission from liquid hydrometeors in the absence of ice-phase cloud (Crewell and Lohart, 2003). The algorithm uses 89 GHz emission and integrated water vapor measurements from the

Advanced Microwave Scanning Radiation –EOS (AMSR-E) and clear-sky sea surface temperatures from the Moderate Resolution Imaging Spectroradiometer (MODIS). Both instruments are onboard the NASA Aqua satellite which was launched in 2002 (King et al. 2003). While MODIS is still operational, AMSR-E data is only available through 2011 due to an instrumentation failure. Horizontally-polarized 89 GHz brightness temperatures are obtained from the AMSR-E Level 2 Brightness Temperature Product (Ashcroft and Wentz 2006). Sea surface temperatures from the MODIS Level 2 Cloud Product (King et al. 2003) are utilized to constrain background emissivity values. Integrated water vapor output from the AMSR-E Ocean Version 6 Product (Wentz and Meissner 2004) is also used to distinguish background emissivity signals. When the algorithm is executed, the final output is a binary heavy drizzle product at ~ 4km x 6km resolution, 1 indicating heavy drizzle (e.g. liquid water path (LWP) > 200 g·m²) at each pixel and 0 indicating no drizzle. Liquid water path in exceedence of 200 g·m² has been validated as an adequate proxy for heavy drizzle (> 0 dBZ) (Zuidema et al. 2005; Kubar et al. 2009). As previously mentioned, this product has a resolution adequate enough to resolve precipitation in heavily-drizzling, individual stratocumulus cells.

The Miller and Yuter (2013) algorithm was evaluated against satellite- and ground-based observations. C-band radar reflectivities greater than 0 dBZ (Comstock et al. 2005) retrieved from the VAMOS Ocean-Cloud-Atmosphere-Land Study field campaign (Wood et al. 2011) consistently match binary output from the 89 GHz algorithm in the SEP (Figure 2.2). Hit and miss statistics derived by comparing linearly-interpolated radar data to the binary output

yielded an average hit rate of 76.8%, an average miss rate of 2.2%, and an average false alarm rate of 21.0%. MODIS liquid water path satellite observations from the NEP and NEA match the binary output. Surface based radar data are not available for these regions during the period of AMSR-E data availability.

Though MODIS-derived liquid water path is a finer spatial resolution (1 km x 1 km) than the Miller and Yuter (2013) product and useful for identifying areas that are likely drizzling, it is only available during the day as visible channels are required. The AMSR-E liquid water path product (14 km x 8 km) has coarser resolution than the Miller and Yuter (2013) product and is therefore unable to adequately resolve individual stratocumulus cells. These datasets are compared with the 89 GHz-based product in Figure 2.3. It is worth emphasizing the usefulness of the 89 GHz-based product as it is available at night and is obtained at a finer resolution (6 km x 4 km) than that of the AMSR-E liquid water path product.

2.3 89 GHz Algorithm Over Terrestrial Surfaces

Limitations of the 89 GHz algorithm are exposed in the SEA and SEP. The algorithm fails over land because of the empirical 89 GHz emissivity threshold. The background emissivity of terrestrial surfaces is more heterogeneous and less easily constrained; tracking precipitation frequencies over land is beyond the utility of this method. Pixels including land masses are excluded from the regional statistics.

2.4 Ancillary Satellite-Derived Cloud Characteristics

In addition to the 89 GHz algorithm output, cloud droplet number concentrations and sea surface temperatures are analyzed in each area of interest. The cloud droplet number concentrations are calculated courtesy of Ralf Bennartz using 1-km MODIS Level 2 Cloud Product cloud effective radii and cloud optical thickness (Platnick et al. 2003). The methodology for calculating these concentrations is documented in Bennartz (2007). Sea surface temperature data is from the Remote Sensing Systems microwave, optimally-interpolated product. This product uses microwave retrievals to run a simple radiative transfer model that estimates sea surface temperatures (Gentemann et al. 2003).

2.5 Data Processing Method

For each region, the Aqua overpass times are approximately 01:30 and 13:30 LST. MODIS files are first filtered using a +/- 3-hour window according to the overpass times in each region. The algorithm is then run for each time step that has a matched MODIS and AMSR-E output time within 120 minutes (data have different temporal resolutions – MODIS files are output in 5-minute granules while AMSR-E files are output in 50-minute orbits). The AMSR-E integrated water vapor product (27 km x 16 km resolution) and MODIS sea surface temperature (5 km x 5 km resolution) arrays are interpolated to 89 GHz product resolution (6 km x 4 km resolution) using the tri-scatter interpolation function available in MATLAB. Further analysis is based upon a set of output arrays that contain the binary drizzle product, interpolated geolocation values, and MODIS cloud top temperature values for each overpass time.

The AMSR-E dataset is available from July 2002 – October 2011, yielding 108 full months of data available for analysis. Satellite data are processed in one-month intervals and aggregated by season. The resulting seasonal aggregates by region have approximately 2000 output files that met the geographic (local time stamp) criteria. The algorithm is processed for the entire AMSR-E dataset to reduce the impact of sampling noise and improve the detection of sub-regional trends (dataset overview provided in Table A1.1).

2.6 Ice-Phase Cloud Mask

The 89 GHz algorithm is tailored specifically for marine stratocumulus clouds which remain in the liquid-phase. The geographic bounds used in this study contain areas where ice-phase cumulus clouds are also prevalent; these areas are removed in order to analyze regions associated with strictly liquid-phase clouds.

Ice-phase cloud frequencies are calculated for seasonal aggregates. The threshold value of 33% was determined based on the spatial extent of the clouds formed in the inter-tropical convergence zone (ITCZ). As such, if a pixel has ice-phase cloud more than 33% of the time during the period of interest, it is excluded from analysis in the seasonal composites. For consistency, the same threshold value is applied to all regions. Increasing this threshold would significantly decrease the area viable for analysis during DJF and MAM in the NEP. Areas recognizably part of the ITCZ would be included in the analysis if the threshold was

decreased. Cloud top temperature distributions are available by region, season, and overpass time in Figures A1.1-A1.3 (Appendix).

Chapter 2 – Figures

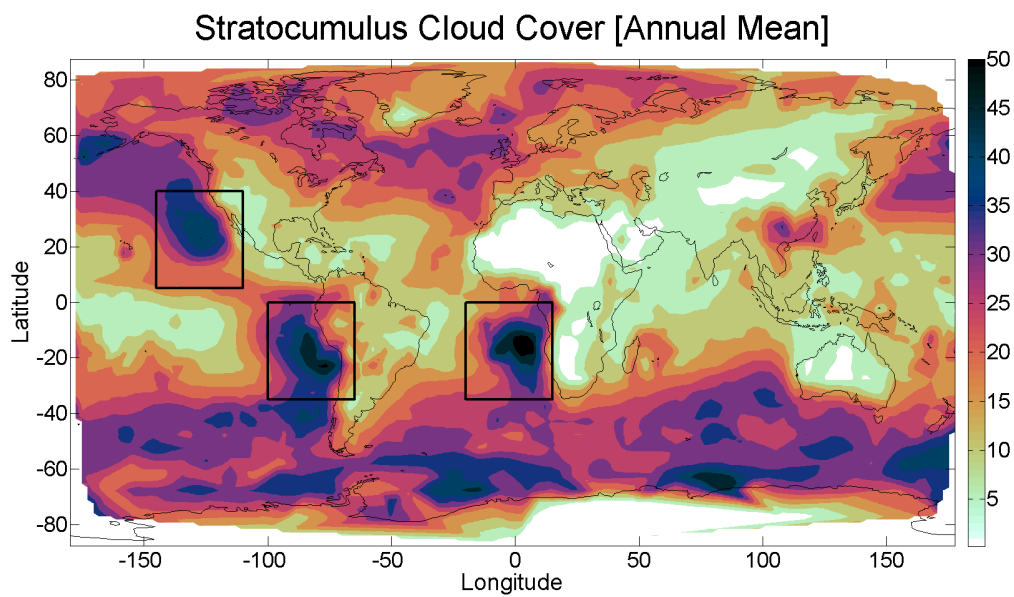


Figure 2.1. Average stratocumulus cloud cover (%) from the Climatic Atlas of Clouds Over Land and Ocean (Hahn and Warren 2007). Marine stratocumulus areas of interest are outlined in black.

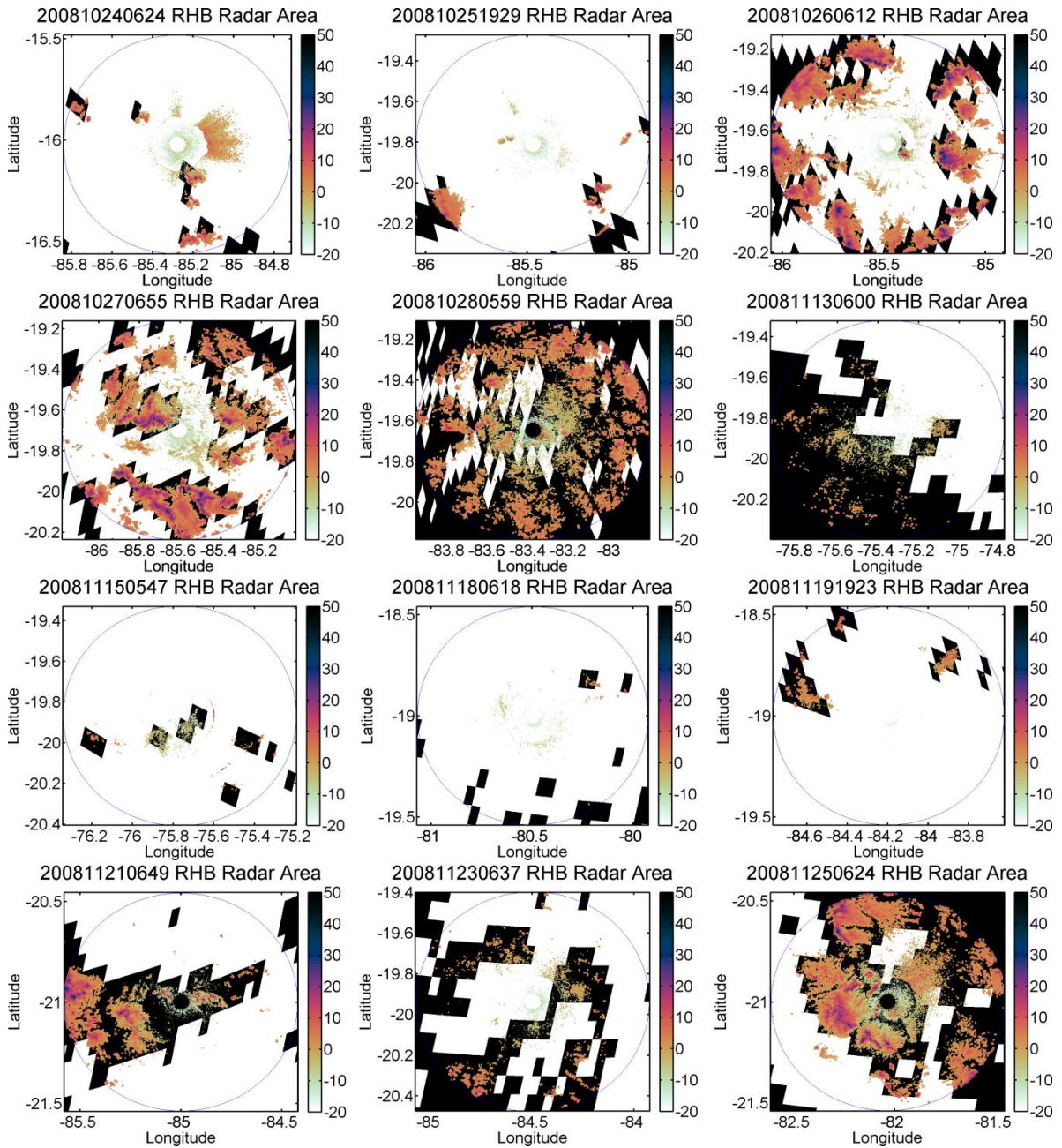


Figure 2.2. C-band radar reflectivities (color scale) from the VOCALS field campaign in the Southeast Pacific during SON 2008 overlaid atop the 89 GHz binary drizzle algorithm (black shading). Figure from Miller and Yuter (2013).

26 June 2007

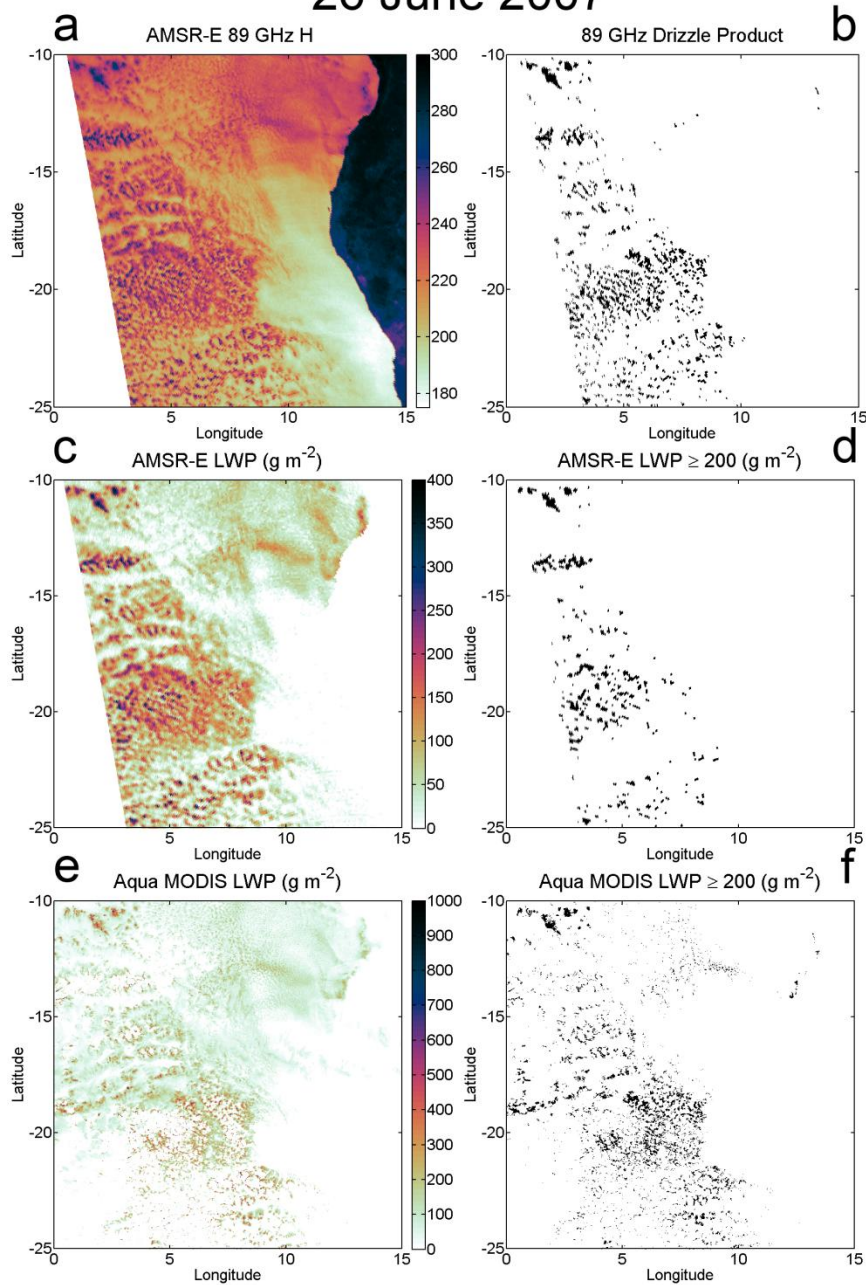


Figure 2.3. Comparison among a) AMSR-E 89 GHz channel output, b) AMSR-E binary drizzle product, c) AMSR-E liquid water path output, and e) MODIS liquid water path output. Liquid water path $> 200 \text{ g}\cdot\text{m}^{-2}$ is shown as a binary product in d) and f). Data are from the Namibian region on 26 June 2007. Figure from Miller and Yuter (2013).

Chapter 3 – Regional Precipitation Frequency Distributions

3.1 Introduction

There are distinct differences between the SEP, NEP, and NEA marine stratocumulus regions. The following sections discuss the spatial and temporal trends in each individual region; the final section in this chapter compares the three regions and postulates possible causes of the marked differences in observed precipitation frequency. In the sections that follow, seasons are referred to by initialisms: December-January-February (DJF), March-April-May (MAM), June-July-August (JJA), and September-October-November (SON). Drizzle frequency peaks in the SEP and NEA during SON and in the NEP during JJA.

Figures 3.1-3.3 represent the observed frequency of precipitation by region, time, and season. The binary output from each output file is aggregated into 55 km x 52 km bins. This bin size is the result of dividing the 35° longitude by 35° latitude region centered off the equator into a 100 x 100 grid. Each bin represents the frequency of pixels that are flagged positive for drizzle within the bin coverage area; bins are normalized with respect to the sample size per bin. The regions shaded in gray (usually in the northern and southern parts of the scene) are not included in the analysis as these areas are zones where the ice-phase cloud frequency exceeded 33%. This threshold value is based on the ice-phase cloud top temperature climatology described in the Section 2.6

The land areas of islands are assigned zero drizzle frequency. As discussed in Section 2.3, the algorithm does not function over land surfaces. Hence, histogram bin grid boxes over islands have artificially diminished drizzle frequencies. In the SEP, the impacted regions are close to the Chilean islands of Desventuradas (26°S, 80°W) and Juan Fernandez (33°S, 79°W). (Figure 3.1). In the SEA, the island of St. Helena (16°S, 8°W) has significantly lower precipitation frequencies than the surrounding areas (Figure 3.3) for the same reason.

3.2 Southeast Pacific

The SEP has a well-documented diurnal signal and east-west precipitation gradient (de Szoeke et al. 2012). The nighttime precipitation frequency is highest during SON (Figure 3.1h), as expected according to boundary layer static stability trends (Klein and Hartmann 1993). Precipitation frequencies during SON exceed 0.3 (30%) - the equivalent of 27 observations of drizzle out of 90 total samples over a three-month period. Nighttime precipitation areas follow a coastal gradient that aligns with the South American coastline and cold-water upwelling zones (Figure 3.1e-h). Higher precipitation frequencies (> 0.25) are constrained between 10°S and 24°S where large-scale subsidence maintains sufficiently shallow boundary layers. The precipitation distributions are displaced northward from DJF (austral summer) to JJA (austral winter) by approximately 2° latitude. There is a northwest to southeast gradient of precipitation evident in all seasons.

Daytime precipitation is most widespread during JJA. Precipitation frequency distributions peak during JJA (Figure 3.1c) and are lowest during DJF (Figure 3.1a). Daytime

precipitation distributions follow the coastline and upwelling zones of colder SST at 17°S (Figure 3.1a-d). During MAM, zones of higher precipitation frequencies are displaced further south.

3.3 Northeast Pacific

The NEP stratocumulus region off the coast of California and Baja California is heavily constrained by the ITCZ in all seasons (Figure 3.2). The ITCZ, indicated by areas shaded in gray where ice-phase clouds are prevalent, is further north during JJA (boreal summer) compared to DJF (austral summer). Nighttime precipitation frequency peaks in JJA (Figure 3.2g) and, as corroborated in Leon et al. 2008, occurs during the season when static stability and cloud coverage maxima occur (Klein and Hartmann 1993). Though nighttime precipitation frequency peaks in JJA, high precipitation frequencies greater than 0.13 are also prevalent in MAM (Figure 3.2f) and SON (Figure 3.2h) between 15°N and 25°N. The region north of 25°N, however, has high precipitation frequency maxima only in JJA. During JJA, the northward displacement of large-scale subsidence associated with the descending branch of the Hadley circulation allows for a more extensive stratocumulus deck and associated precipitation fields. Nighttime precipitation frequency is lowest during DJF (Figure 3.2e).

Between 15°N and 25°N during JJA and SON (Figure 3.2c-d) there is a distinguishable area of higher daytime precipitation frequencies (0.1) not evident during DJF and MAM (Figure 3.2a-b). The region north of 25°N has a subtle daytime precipitation frequency maxima during SON (Figure 3.2d). It is notable that nighttime and daytime precipitation frequency

maxima do not occur during the same season. A monthly breakdown of precipitation frequency, feasible using this dataset, is beyond the scope of this study and will be the subject of future investigations.

Documentation of areas where mid-latitude cumulus and cirrus clouds are common more than 33% of the time is a residual product of this climatology (Figures A1.1-A1.3). Shaded areas north of 30°N during DJF and MAM (Figure 3.2a-b) indicate areas where ice-phase cloud dominates due to the synoptic forcings and jetstream dynamics. The low-level cloud field expands northward during JJA and SON (Figure 3.2c-d). The shaded ice-phase cloud mask exposes a well-defined ITCZ during JJA and SON. During DJF and MAM spatial inhomogeneity in the ice-phase cloud field is apparent from 10° – 20° N. The northeastward band of ice-phase cloud mask from 130°W – 142°W during MAM (Figure 3.2f) and from 110°W – 130°W during DJF (Figure 3.2a,e) is the subject of future inquiry.

3.4 Southeast Atlantic

The SEA stratocumulus region is constrained by the southeastward shift of the ITCZ during DJF and MAM and the mid-latitude, mixed-phase cloud environment south of 30°S during MAM, JJA, and SON (Figure 3.3). During JJA and SON there is a north-south gradient across 16°S. This gradient is collocated with the slight bight that occurs at the Angolan/Namibian border at 17°S. This gradient is also associated with an underwater ridge that creates a localized region of cooler sea surface temperatures. Nighttime precipitation frequency peaks in SON (Figure 3.3h) but also has high values (> 0.17) during JJA (Figure

3.3f). The area within 7°S-15°S and 5°W-15°W has continuous precipitation frequencies that exceed 0.2 during SON; this value is not replicated in any other season in the SEA. During SON, static stability maxima and cloud coverage peaks in this area (Klein and Hartmann 1993). Similar to the other two regions of interest, precipitation distributions exhibit an east-west gradient along the coast line most prominent during MAM, JJA, and SON (Figure 3.3f-h). The east-west gradient is likely due in part to coastal jet dynamics and shoaling that confine the boundary layer (and reduce precipitation efficiency) closer to the African coastline (Zuidema et al. 2009). During DJF and MAM (Figure 3.3e-f) there are too many clouds with ice to determine drizzle frequency in the area north of 16°S and east of 5°E. The ITCZ (and associated tropical, high-level cumulus clouds depicted by the gray shaded areas) and implicated convergence fields slope northeastward between MAM and SON (Figure 3.3f,h). As a result, subsidence fields are displaced and the zone of liquid-phase cloud and seasonal nighttime precipitation maxima shift northward and westward from 15°S-25°S/2°E-10°W in MAM to 7°S-15°S/5°W-15°W in SON.

An east-west coastal gradient is apparent in the composites of daytime precipitation frequency (Figure 3.3a-d). The precipitation field shifts north from MAM to SON (Figure 3.3b,d). The daytime precipitation field is most widespread during JJA (Figure 3.3c), consistent with the low-cloud climatology (Hahn and Warren 2007). The gradient of precipitation follows the coastline contour (particularly during JJA and SON). Daytime precipitation frequency is lowest during DJF (Figure 3.3a).

3.5 Regional Contrasts

Each region has markedly different precipitation frequency distributions by season and time. The SEP has the highest variation between daytime and nighttime scenes compared to the SEA and NEP (Figures 3.1 – 3.3). All three regions have a distinct coastal gradient of precipitation due to coastal shoaling (Zuidema et al. 2009). Unlike in the SEP, daytime precipitation frequency in the NEP does not have a clear seasonal peak (Figure 3.2a-d).

Distributions of cloud top temperature and drizzle occurrence point to subtle differences among the three regions of interest (Figures 3.4,3.5). The modal cloud top temperature is lowest in the SEP at night and highest in the NEP during the day (Figure 3.4). Further analysis and more ice-phase cloud filtering is needed to infer whether this indicates an overall deeper boundary layer in the SEP compared to other regions. Distributions of scene drizzle fraction during the peak season suggest that the SEP has the widest distribution of scene drizzle frequency and has a higher scene-by-scene precipitation occurrence (Figure 3.5).

Chapter 3 – Figures

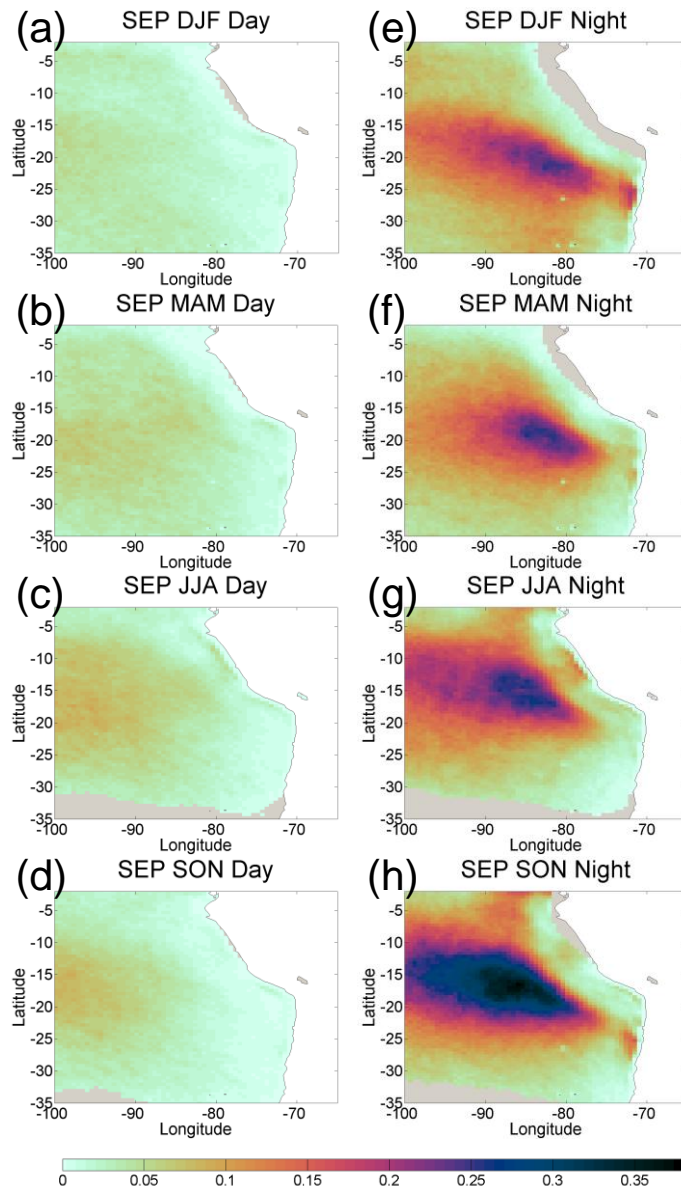


Figure 3.1. Spatial distributions of liquid-phase precipitation frequency (pixels where 89 GHz binary drizzle product = 1) for the Southeast Pacific by season and time during the AMSR-E operational period from 2002-2011. The colorbar indicates fractional drizzle frequency. Frequencies are normalized by sample size per bin. The area shaded in gray exceeds the ice-phase cloud frequency threshold (>33%).

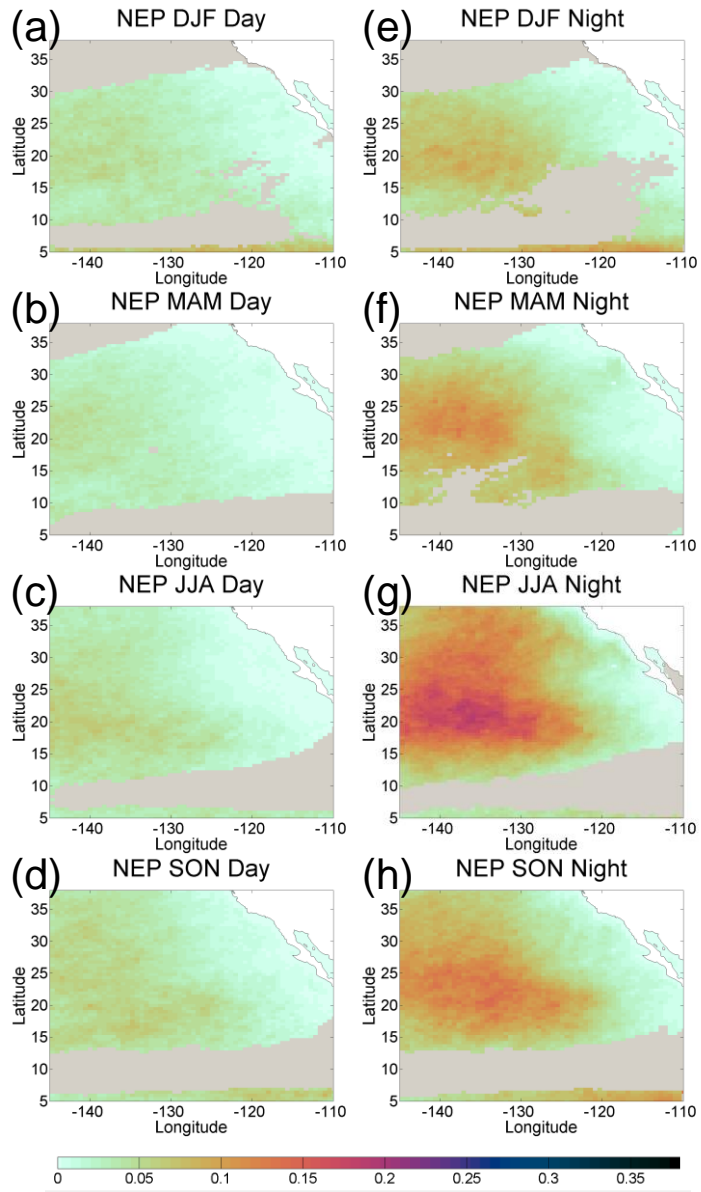


Figure 3.2. As in Figure 3.1 but for the Northeast Pacific.

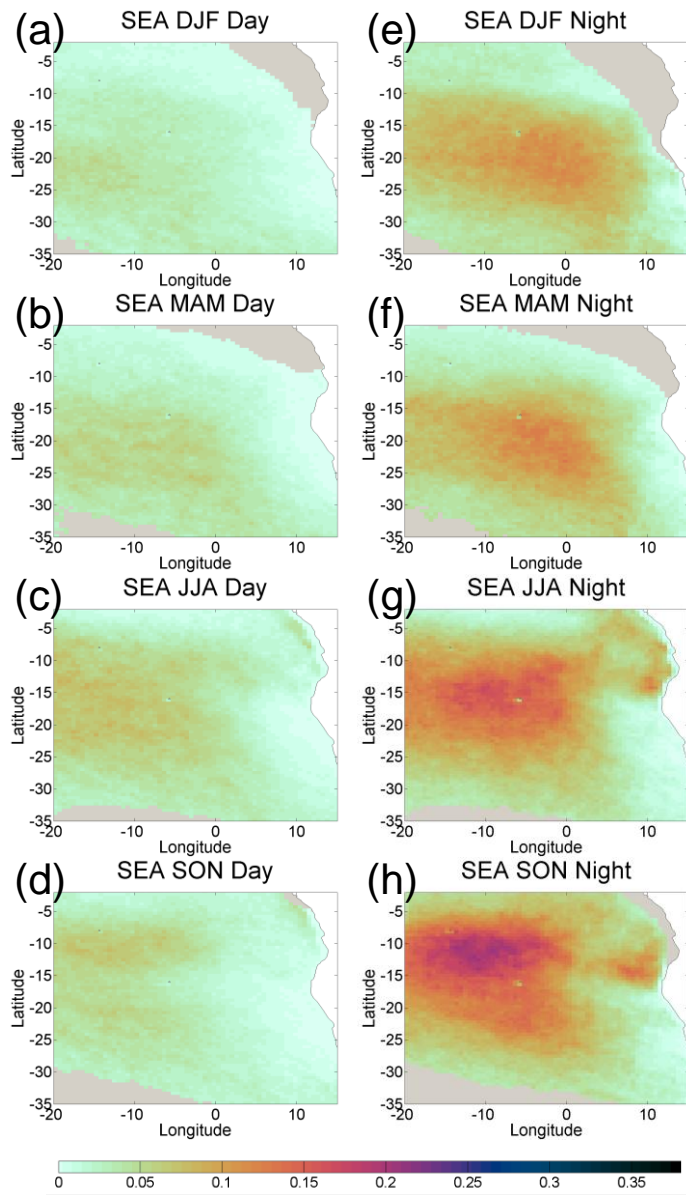


Figure 3.3. As in Figure 3.1 but for the Southeast Atlantic.

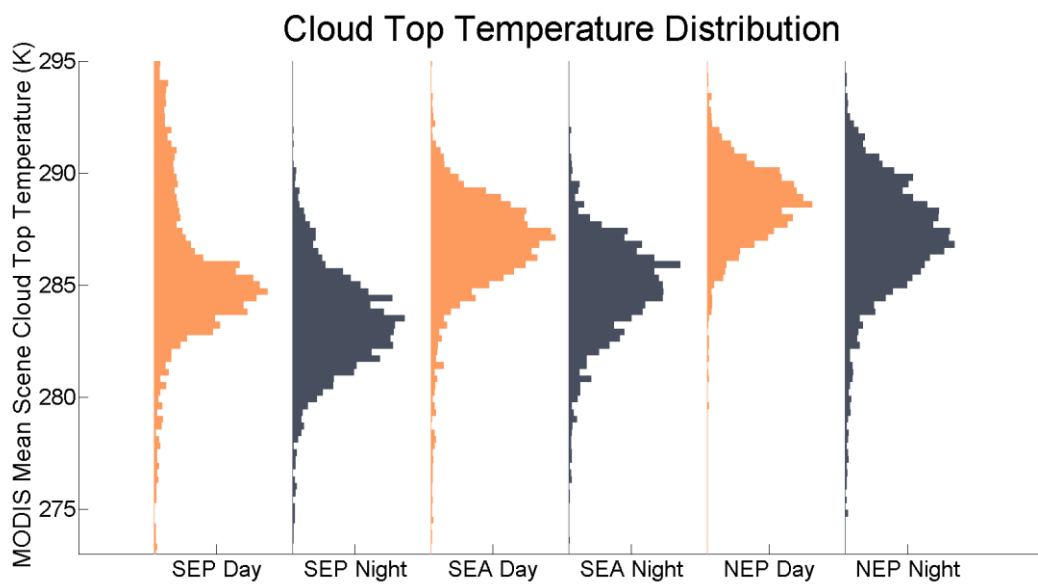


Figure 3.4. Distributions of liquid-phase cloud top temperature by region and time for the season with the highest drizzle occurrence (SON in SEP and SEA; JJA in NEP).

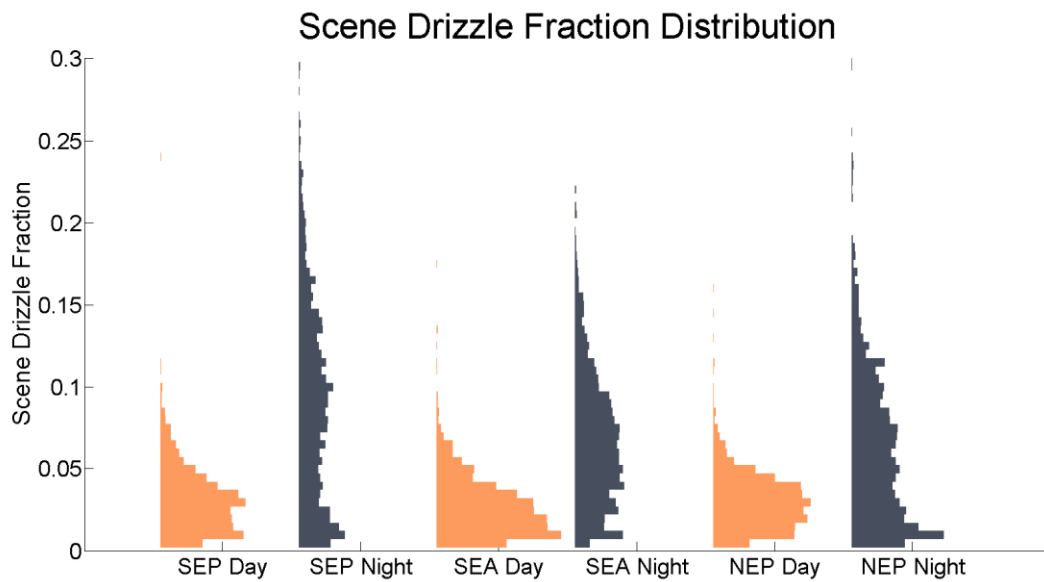


Figure 3.5. Distributions of drizzle fraction per scene by region and time for the season with the highest drizzle occurrence (SON in SEP and SEA; JJA in NEP). A scene is one file that corresponds to a MODIS overpass time. There is no scene during this time with a drizzle fraction of zero.

Chapter 4 – Interannual Precipitation Trends and Comparisons Among Regions

In this section, the interannual variability of heavy drizzle frequency is examined for each of the three 35° x 35° marine stratocumulus regions. For each three-month season in a given year, the number of 55 km x 52 km bins with precipitation frequency values exceeding a threshold value are multiplied by average bin area (2878 km²). The day and night drizzle area data are presented chronologically as bar plots in Figure 4.1. For illustration purposes, the frequency thresholds of 0.07, 0.1, 0.2, and 0.3 were determined based on an evaluation of spatial trends and maxima. The minimum frequency threshold was set at 0.07 because drizzle frequencies below this threshold consistently occur on the outer edges of the areas of interest. Figure 4.1 illustrates the annual cycle of heavy drizzle area as well as year-to-year variations. The frequency threshold values by year and region for the season when drizzle is most prevalent are available in Appendix Tables A1.2-A1.7.

Further detail about the nature of the interannual variability is provided in Figures 4.2 and 4.3 which showcase the drizzle frequency composites for the pair of years with the largest difference in drizzle area during the peak season. The complete set of seasonal drizzle frequency composites by year is available in the Appendix (Figures A1.4-A1.7).

As noted in Chapter 3, during their respective peak seasons, SEP has a larger area of heavy drizzle than either SEA or NEP. The SEP also has the largest area where the precipitation frequency is greater than 0.3 (indicated by dark purple in Figure 3.1e-h). Of the three

geographic areas during their respective peak drizzle season, NEP has the lowest total nighttime precipitating area (Figure 4.1d), the highest interannual range (JJA - $3.06 * 10^6$ km²), and the largest standard deviation of precipitating area by season (JJA - $1.00 * 10^6$ km²). The largest interannual range in daytime precipitation frequency during the peak season is in the SEA (SON - 952,000 km²) while the largest standard deviation is in the SEP (SON - 302,000 km²) (Figures 4.1a,c).

Environmental controls on minimum daytime and nighttime precipitation areas during peak drizzle season have interannual cycles that vary by geographic region. Two years stand out over the 2002-2011 period, 2010 and 2002. The SEP and NEP both have nighttime precipitating area maxima in 2010 (Figure 4.2d,e). The NEP has daytime precipitating area maxima in 2010 as well (Fig. 4.3e). The timing of this maxima may infer a linkage between a low El Nino Southern Oscillation (ENSO) and conditions favorable for heavy drizzle formation in the subtropical Pacific. From 2002-2011, the ENSO index was lowest during the 2010 season. Colder oceanic temperatures are associated with low ENSO indices. Colder boundary layers are shallower and easily mixed; this provides a more favorable environment for surface-cloud base interactions. For a given region, NEP and SEA have maximum day and night values in the same year (2006). The year 2002 corresponds to daytime minima in drizzle area in the SEP and SEA as well as nighttime minima in SEA. NEP has drizzle area minimum for both day and night in 2009. Overall, large scale environmental controls on drizzle formation appear to be complex and will be the subject of future work.

Chapter 4 - Figures

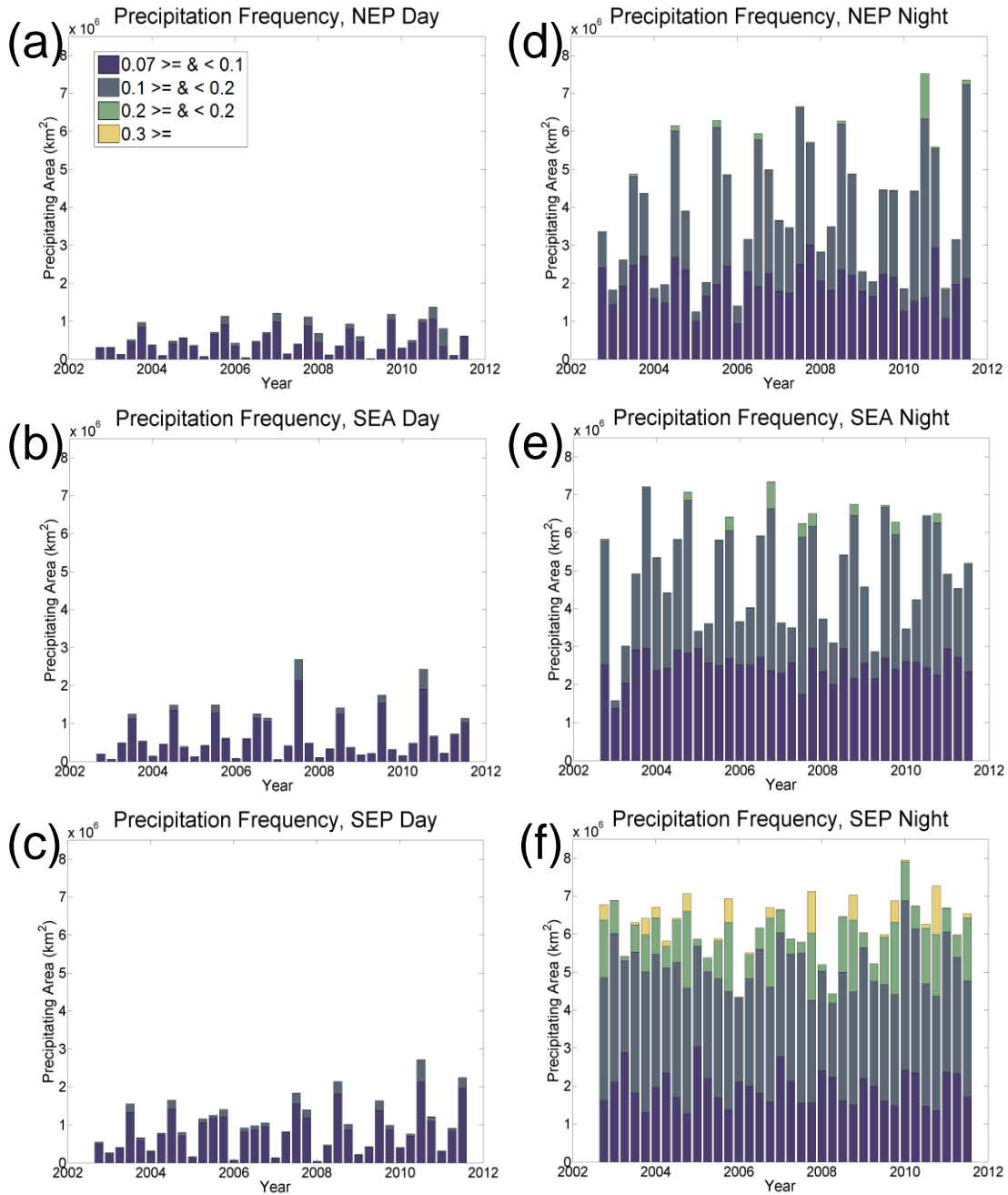


Figure 4.1. Total drizzle area is aggregated by season, region, and overpass time. Precipitation frequency area is calculated by multiplying the bins meeting a threshold frequency by the average bin size (2878 km²).

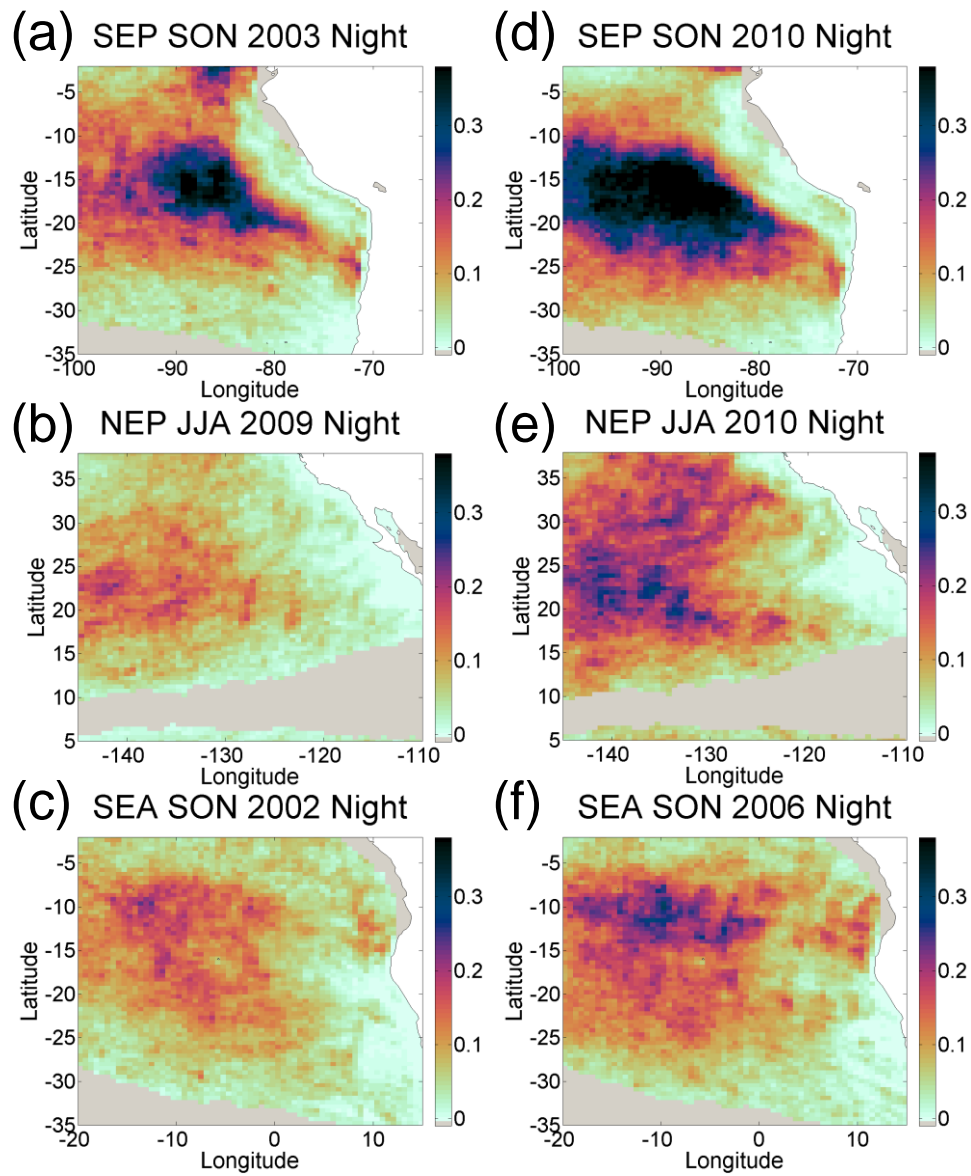


Figure 4.2. Distributions of precipitation frequency for the years when precipitation frequency was minimized (a-c) and maximized (d-f) during the season when precipitation is most prevalent.

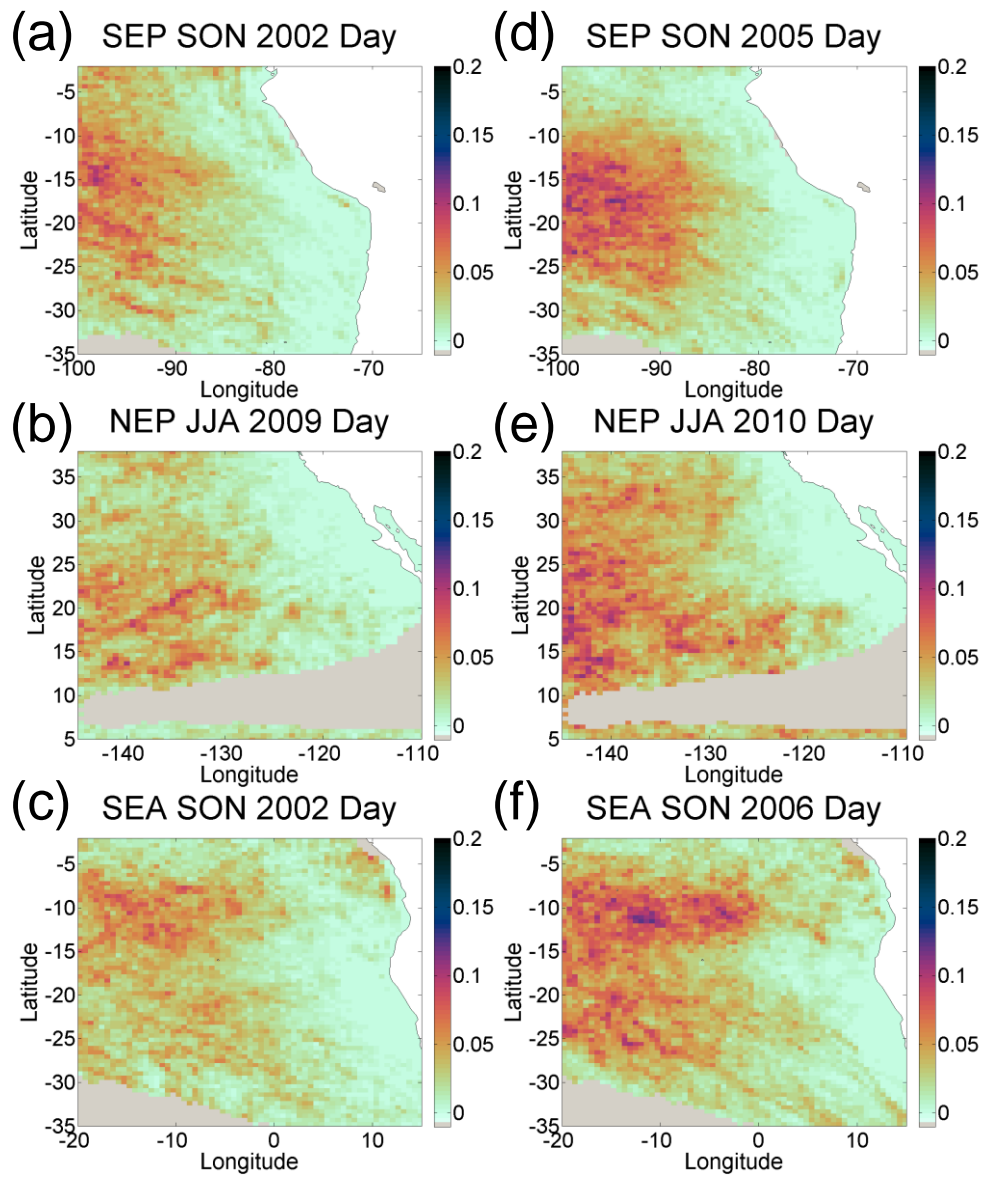


Figure 4.3. As in Figure 4.2 but for daytime distributions.

Chapter 5 – Comparison of Regional Environmental Parameters

In this chapter, two potential environmental sources of drizzle variability are examined – SST and cloud droplet number concentration. Higher sea surface temperatures are associated with higher boundary layers and increased likelihood of drizzle (de Szoeke et al. 2012; Mechem et al. 2012; Wood 2012; Burleyson et al. 2013). Cloud droplet number concentration is also a strong control on the formation of drizzle as higher number concentrations are associated with smaller cloud droplets and less probability of drizzle formation (Albrecht 1989; Mechem et al. 2012). In this section, we use the Bennartz (2007) cloud droplet number concentration (CDNC) product which is derived from MODIS data. Only CDNC data from 2003-2004 were available from Bennartz (personal communication). Maps of the average precipitation frequency, sea surface temperatures, and cloud droplet number concentration from the 2003 and 2004 seasons are presented in Fig. 5.1. The areas in the CNDC maps that are shaded in gray did not meet the threshold for Bennartz's analysis as the cloud fraction was too low (Figure 5.1g-i). Overall, drizzle frequency increases westward away the coasts as SST tends to increase and CDNC tends to decrease. Both sea surface temperature and CDNC fields have some spatial correlation with drizzle frequency patterns but neither variable appears to be a dominate control (Figure 5.2). It is worth noting, however, that CDNC values greater than 100 cm^{-3} appear to be a 'switch' for heavy drizzle.

The CDNC values are very high along the coasts of all three regions as anthropogenic emissions are most prevalent there. It is well understood that coastal emissions (e.g. smelters, biomass burning) act to influence cloud formation in all three regions (Zuidema et

al. 2009). Depending on the specific values of cloud condensation nuclei (CCN) concentrations used, LES modeling has indicated that higher CCN concentrations can suppress or delay drizzle (Stevens et al. 2005; Wang and Feingold 2008; Mechem et al. 2012). Our observations indicate that higher cloud droplet number concentrations ($> 130 \text{ cm}^{-3}$) decrease the probability of drizzle by the coast but do not suppress it completely. An important question is whether SST (e.g. boundary layer height) or CDNC is a stronger control on heavy drizzle formation (Mechem et al. 2012). If one or the other was the dominant control one would expect drizzle frequency of occurrence to follow any sharp gradients in SST or CDNC.

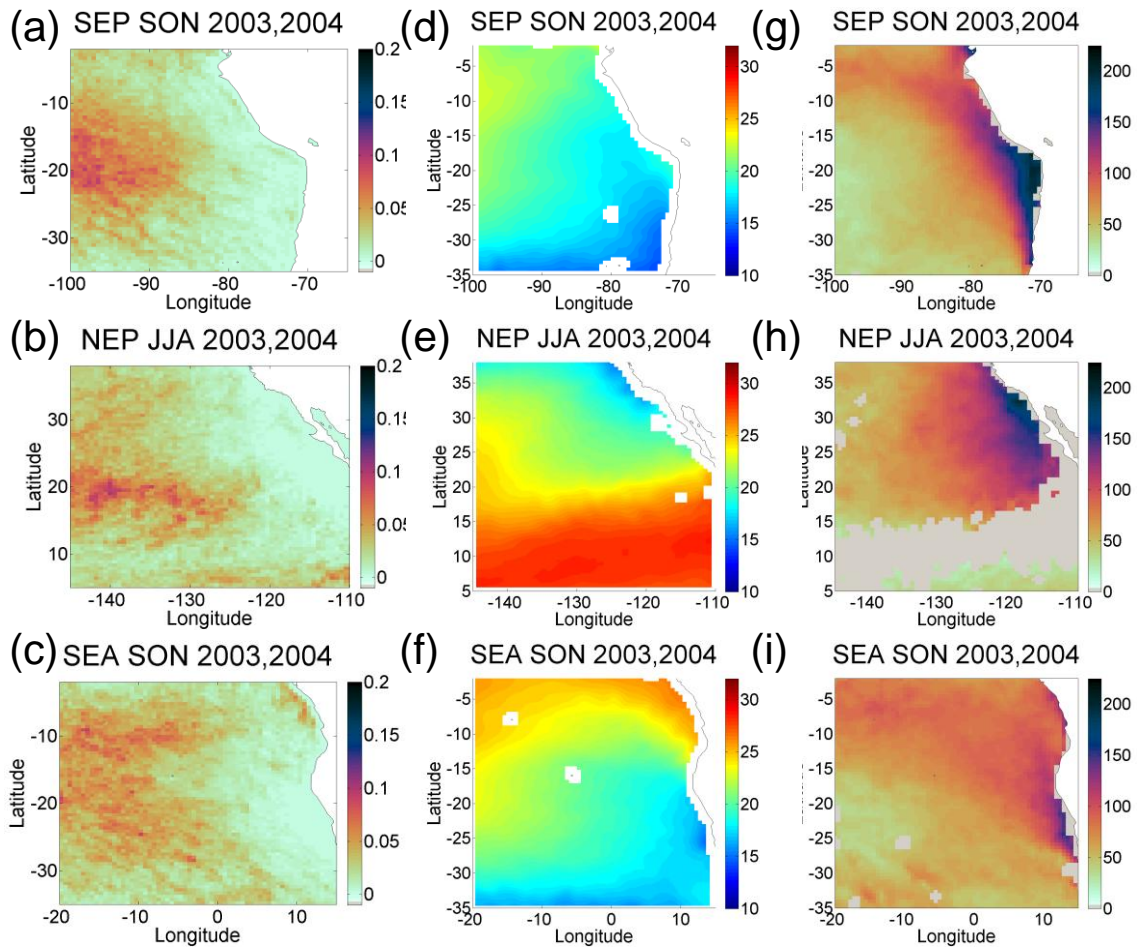


Figure 5.1. Distributions of the 89 GHz precipitation frequency (a-c), optimally-interpolated sea surface temperatures (d-f), and cloud droplet number concentrations (g-i). All distributions are averaged over the 2003 and 2004 seasons. Areas in gray in the precipitation distributions (a-c) are shaded because ice-phase cloud frequency was too high (>33%). Areas in gray in the cloud droplet number concentrations (g-i) are shaded because cloud fraction was too low (<0.4).

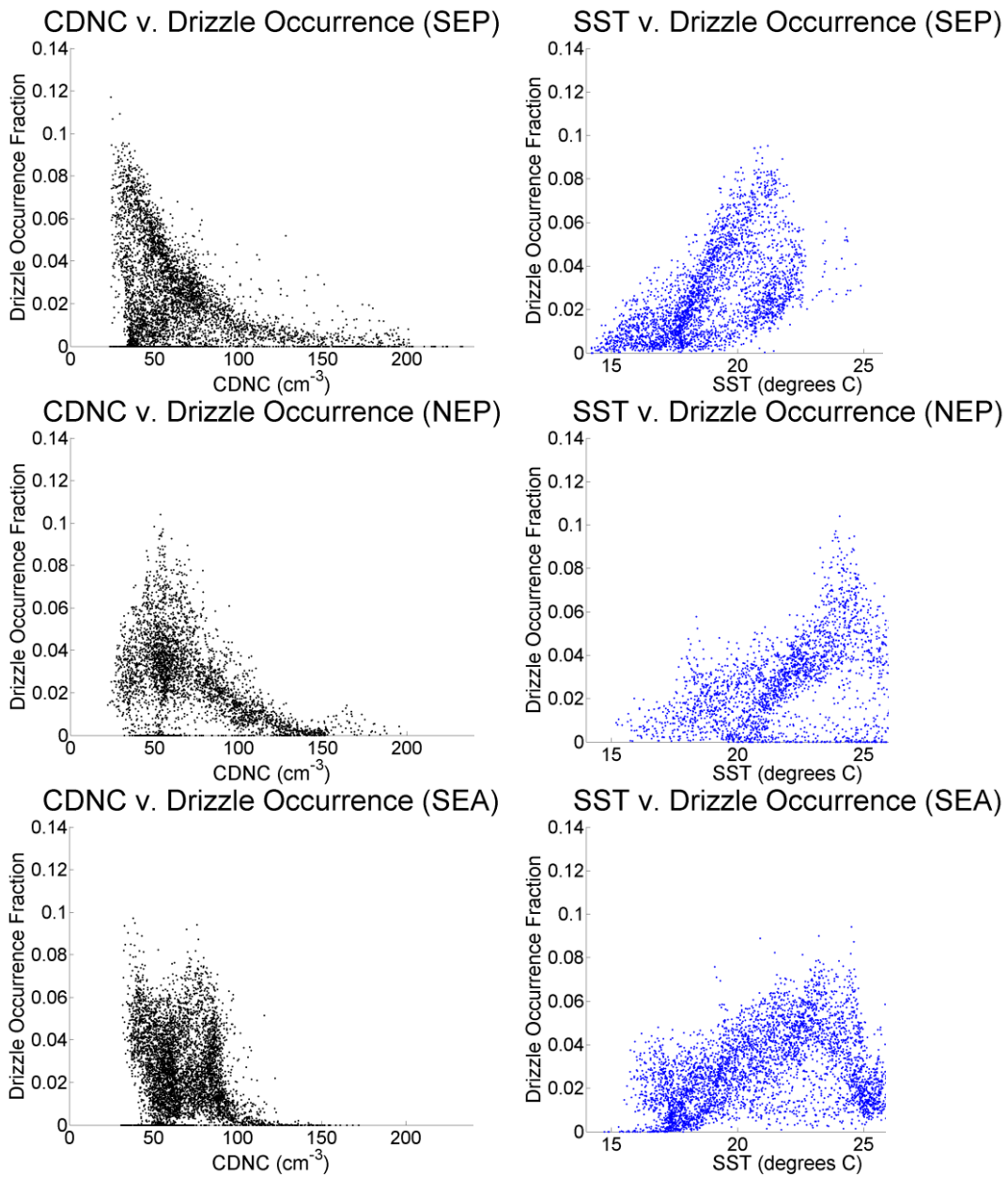


Figure 5.2. Comparison of cloud droplet number concentrations and sea surface temperature fields with drizzle occurrence by region during the season when drizzle occurrence is highest. Data only available during the day for the 2003-2004 seasons.

Chapter 6 – Conclusions

6.1 Discussion

Marine stratocumulus precipitation is a ubiquitous feature in all three areas of interest. This work is the first to combine an examination of marine stratocumulus diurnal and interannual variability of drizzle occurrence with a comparison among the three main marine stratocumulus geographic regions. There is a marked diurnal cycle in precipitation associated with variations in shortwave radiative fluxes (Leon et al. 2008; Burleyson et al. 2013). Of the three regions, the SEP has the highest frequency of drizzle occurrence in both night and day. The NEP and SEA do not have precipitation frequencies that exceed 30% as found in the SEP at night. In the SEP(NEP), drizzle occurrence at night was highest in SON(JJA) of 2010 corresponding to a La Nina event (cold SSTs in central equatorial Pacific). The interannual minima in frequencies coincided for day and night for the NEP and SEA but not for the SEP.

The environmental parameters that favor precipitation formation are complex and numerous. Importance has been placed by various research communities on every meteorological scale – be it large-scale subsidence fields to cloud microphysical processes. The most obvious linkage to precipitation occurrence is sea surface temperature as this variable influences boundary layer depth and modulates surface-cloud base interactions (and corresponding moisture fluxes). Both sea surface temperature and cloud droplet number concentration fields have some spatial correlation with drizzle frequency patterns but neither variable appears to be a dominate control. Cloud droplet number concentrations greater than 100 cm-

3 appear to be a 'switch' for heavy drizzle. Very high cloud droplet number concentrations ($> 130 \text{ cm}^{-3}$) close to the coast decrease the probability of heavy drizzle occurrence but do not suppress it entirely.

6.2 Future Work

Future work will explore the linkages between drizzle occurrence and other environmental factors such as large-scale subsidence, lower tropospheric static stability, cloud fraction, and radiative flux. Now that precipitation frequency appears to be more nuanced and variable for each region of interest it will be important to compare and contrast the environmental regimes of the three regions as the controlling factors may prove slightly different. The author is also interested in a more robust statistical analysis of interannual high-frequency precipitation area and in exploring the factors that control the diurnal variability, particularly in the SEP. The data produced in this study can also be used to study some aspects of mesoscale precipitation organization as the resolution is fine enough to detect larger individual precipitation cells.

References

- Ackerman, A. S., O. B. Toon, and P. V. Hobbs, 1993: Dissipation of marine stratiform clouds and collapse of the marine boundary layer due to the depletion of cloud condensation nuclei by clouds. *Science*, **262**, 226–229.
- Albrecht, B.A., 1989: Aerosols, Cloud Microphysics, and Fractional Cloudiness. *Science*, **245**, 1227–30.
- Ashcroft, P. and F. Wentz, 2006: AMSR-E/Aqua L2A Global Swath Spatially-Resampled Brightness Temperatures V002, Various dates, <http://www.nsidc.org/data/amsre>, National Snow and Ice Data Center, Boulder, Colorado, USA.
- Atkinson, B. W., and J. W. Zhang, 1996: Mesoscale shallow convection in the atmosphere. *Rev. Geophys.*, **34**, 403–431.
- Bennartz, R., 2007: Global assessment of marine boundary layer cloud droplet number concentration from satellite. *J. Geophys. Res.*, **112**, D02201, doi:10.1029/2006JD007547.
- Berner, A. H., Bretherton, C. S., and Wood, R., 2011: Large-eddy simulation of mesoscale dynamics and entrainment around a pocket of open cells observed in VOCALS-REx RF06, *Atmos. Chem. Phys.*, **11**, 10525-10540, doi:10.5194/acp-11-10525-2011.
- Bretherton, C.S., T. Uttal, C. W. Fairall, S. E. Yuter, R. A. Weller, D. Baumgardner, K. Comstock, and R. Wood, 2004: The EPIC 2001 stratocumulus study. *Bull. Amer. Meteor. Soc.*, **85**, 967–977.
- Burleyson, C. D., S. P. deZoeke, S. E. Yuter, M. Wilbanks, and W. A. Brewer, 2013: Observations of the diurnal cycle of southeast Pacific marine stratocumulus clouds and precipitation. *J. Atmos. Sci.*, submitted 12/12.
- Clement, A.C., R. Burgman, and J.R. Norris, 2009: Observational and model evidence for positive low-level cloud feedback. *Science*, **32**, 460–464.

Comstock, K. K., R. Wood, S. Yuter, and C. S. Bretherton, 2004: Radar observations of precipitation in and below stratocumulus clouds. *Quart. J. Roy. Meteor. Soc.*, **130**, 2891–2918.

Comstock, K. K., C. S. Bretherton, and S. E. Yuter, 2005: Mesoscale Variability and Drizzle in Southeast Pacific Stratocumulus. *J. Atmos. Sci.*, **62**, 3792–3807.

Comstock, K. K., S. E. Yuter, R. Wood, and C. S. Bretherton, 2007: The three-dimensional structure and kinematics of drizzling stratocumulus. *Mon. Wea. Rev.*, **135**, 3767–3784.

Crewell, S. and U. Lohmert, 2003: Accuracy of cloud liquid water path from ground-based microwave radiometry 2. Sensor accuracy and synergy. *Radio Sci.*, **38**, 8042, doi:10.1029/2002RS002634.

de Szoeke, S. P., S. E. Yuter, D. B. Mechem, C. W. Fairall, C. D. Burleyson, and P. Zuidema, 2012: Observations of stratocumulus clouds and their effect on the eastern Pacific surface heat budget along 20°S, *J. Climate*, **25**, 8542-8567.

Eastman, R., S.G. Warren, and C. J. Hahn, 2011: Variations in Cloud Cover and Cloud Types over the Ocean from Surface Observations, 1954–2008. *J. Climate*, **24**, 5914–5934.

Feingold, G., W. Cotton, B. Stevens, and A. S. Frisch, 1996: The relationship between drop in-cloud residence time and drizzle production in numerically simulated stratocumulus clouds. *J. Atmos. Sci.*, **53**, 1108–1122.

Feingold, G., I. Koren, H. Wang, H. Xue, and W. A. Brewer, 2010: Precipitation-generated oscillations in open cellular cloud fields. *Nature*, **466**, 849–852, doi:10.1038/nature09314.

Gentemann, C.L, C.J. Donlon, A. Stuart-Menteth, and F.J. Wentz, 2003:Diurnal signals in satellite sea surface temperature measurements, *Geophys. Res. Lett.*, **30**, 1140-1143.

Ghate, V. P., B. A. Albrecht, C. W. Fairall, and R. A. Weller, 2009: Climatology of surface meteorology, surface fluxes, cloud fraction and radiative forcing over south-east Pacific from buoy observations. *J. Climate*, **22**, 5227-5540.

Hahn, C. J., and S. G. Warren, 2007: A gridded climatology of clouds over land (1971–96) and ocean (1954–97) from surface observations worldwide. Numeric Data Package NDP-026E ORNL/CDIAC-153, CDIAC, Department of Energy, Oak Ridge, TN.

Klein, S.A., and D. L. Hartmann, 1993: The seasonal cycle of low strati-form clouds. *J. Climate*, **6**, 1588–1606.

King, M.D., S.C. Tsay, S. E. Platnick, M. Wang, and K.-N. Liou, 1997: Cloud retrieval algorithms for MODIS: Optical thickness, effective particle radius, and thermodynamic phase. MODIS Algorithm Theoretical Basis Document ATBD-MOD-05, NASA, 78 pp.

King, M. D. and Coauthors, 2003: Cloud and aerosol properties, precipitable water, and profiles of temperature and water vapor from MODIS. *IEEE T. Geosci. Remote*, **41**, 442–458, doi:10.1109/TGRS.2002.808226.

Kubar, T. L., D. L. Hartmann, and R. Wood, 2009: On the importance of macrophysics and microphysics for precipitation in warm clouds. Part I: Satellite observations. *J. Atmos. Sci.*, **66**, 2953–2972.

Lenschow, D.H., I. Paluch, A.R. Bandy, R. Pearson, S.R. Kawa, C.J. Weaver, B.H. Juebert, J.G. Kay, D.C. Thornton, and A.R. Driedger, 1988: Dynamics and Chemistry of Marine Stratocumulus (DYCOMS) Experiment. *Bull. Amer. Meteor. Soc.*, **69**, 1058-1067.

Leon, D. C., Z. Wang, and D. Liu, 2008: Climatology of drizzle in marine boundary layer clouds based on 1 year of data from CloudSat and Cloud-Aerosol Lidar and Infrared Pathfinder Satellite Observations (CALIPSO). *J. Geophys. Res.*, **113**, D00A14, doi:10.1029/2008JD009835.

Mechem, D. B., S. E. Yuter, and S. P. de Szoeke, 2012: Thermodynamic and aerosol controls in southeast Pacific stratocumulus. *J. Atmos. Sci.*, **69**, 1250-1266.

Medeiros, B., D. L. Williamson, C. Hannay, and J. G. Olson, 2012: Southeast Pacific Stratocumulus in the Community Atmosphere Model. *J. Climate*, **25**, 6175–6192.

- Miller, M. A. and S. E. Yuter 2013: Detection and characterization of heavy drizzle cells within subtropical marine stratocumulus using AMSR-E 89-GHz passive microwave measurements, *Atmos. Meas. Tech.*, **6**, 1-13, doi:10.5194/amt-6-1-2013.
- Mitchell, T. P., and J. M. Wallace, 1992: The annual cycle in equatorial convection and sea surface temperature. *J. Climate*, **5**, 1140–1156.
- Pawlowska, H., and J. L. Brenguier, 2003: An observational study of drizzle formation in stratocumulus clouds for general circulation model (GCM) parameterizations. *J. Geophys. Res.*, **108**, 8630, doi:10.1029/2002JD002679.
- Platnick, S., and Coauthors, 2003.: The MODIS cloud products: Algorithms and examples from Terra. *IEEE Trans. Geosci. Rem. Sens.*, **41**, 459–473.
- Randall, D.A., J. A. Coakley, C. W. Fairall, R. A. Knopfli, and D. H. Lenschow, 1984: Outlook for research on marine subtropical stratocumulus clouds. *Bull. Amer. Meteor. Soc.*, **65**, 1290–1301.
- Richter, I., and C. R. Mechoso, 2004: Orographic influences on the annual cycle of Namibian stratocumulus clouds. *Geophys. Res. Lett.*, **31**, L24108, doi:10.1029/2004GL020814.
- Richter, I., and C. R. Mechoso, 2006: Orographic influences on subtropical stratocumulus. *J. Atmos. Sci.*, **63**, 2585–2601.
- Stevens, B., G. Vali, K. K. Comstock, R. Wood, M. VanZanten, P.H. Austin, C. S. Bretherton, and D. H. Lenschow, 2005: Pockets of open cells (POCs) and drizzle in marine stratocumulus. *Bull. Amer. Meteor. Soc.*, **86**, 51–57.
- Stevens, B., A. Beljaars, S. Bordoni, C. Holloway, M. Kohler, S. Krueger, V. Savic-Jovcic, and Y. Y. Zhang, 2007: On the structure of the lower troposphere in the summertime stratocumulus regime of the northeast Pacific. *Mon. Wea. Rev.*, **135**, 985–1005.
- Stevens, B. and Coauthors, 2003: Dynamics and Chemistry of Marine Stratocumulus—DYCOMS II. *Bull. Amer. Meteor. Soc.*, **84**, 579–593.

Suzuki, K., G. L. Stephens, S. C. van den Heever, and T. Y. Nakajima. (2011) Diagnosis of the Warm Rain Process in Cloud-Resolving Models Using Joint CloudSat and MODIS Observations. *J. Atmos. Sci.*, **68**, 2655-2670.

Terai, C., 2011: Drizzle and the aerosol indirect effect in marine stratocumulus. Thesis, Department of Atmospheric Sciences, University of Washington, 91 pp.

Wang, H., and G. Feingold, 2009: Modeling Mesoscale Cellular Structures and Drizzle in Marine Stratocumulus. Part I: Impact of Drizzle on the Formation and Evolution of Open Cells. *J. Atmos. Sci.*, **66**, 3237–3256.

Wentz, F. and T. Meissner, 2004: AMSR-E/Aqua L2B Global Swath Ocean Products Derived from Wentz Algorithm V002, various dates, <http://www.nsidc.org/data/amsre>, National Snow and Ice Data Center, Boulder, Colorado, USA.

Wood, R., 2012: Stratocumulus Clouds. *Mon. Wea. Rev.*, **140**, 2373–2423.

Wood, R. and D. L. Hartmann, 2006: Spatial variability of liquid water path in marine boundary layer clouds: The importance of mesoscale cellular convection. *J. Climate*, **19**, 1748–1764.

Wood, R., K. K. Comstock, C. S. Bretherton, C. Cornish, J. Tomlinson, D. R. Collins, and C. Fairall, 2008: Open cellular structure in marine stratocumulus sheets. *J. Geophys. Res.*, **113**, D12207, doi:10.1029/2007JD009371.

Wood, R., C. Bretherton, D. Leon, A. Clarke, P. Zuidema, G. Allen, and H. Coe, 2011: An aircraft case study of the spatial transition from closed to open mesoscale cellular convection over the southeast Pacific. *Atmos. Chem. Phys.*, **11**, 2341–2370.

Wood, R. and Coauthors, 2011: The VAMOS Ocean-Cloud-Atmosphere-Land Study Regional Experiment (VOCALS-REx): Goals, platforms, and field operations. *Atmos. Chem. Phys.*, **11**, 627–654.

Zuidema, P., E. R. Westwater, C. Fairall, and D. Hazen, 2005: Ship-based liquid water path estimates in marine stratocumulus. *J. Geophys. Res.*, **110**, D20206, doi:10.1029/2005JD00583.

Zuidema, P., D. Painemal, S. de Szoeki, and C. Fairall, 2009: Stratocumulus cloud top estimates and their climatic implications, *J. Clim.*, **22**,4652–4666, doi:10.1175/2009JCLI2708.1.

APPENDIX

Table A1.1. MODIS and AMSR-E dataset overview.

File Count Totals		
MODIS File Count	944784	
AMSR-E File Count	95904	
ScDrizzle Output Files		
Region/Season	# of Files	
NEP	Day	Night
DJF	1496	2224
MAM	1535	2278
JJA	1534	2276
SON	1463	2175
SEP		
DJF	2182	2168
MAM	2232	2224
JJA	2178	2174
SON	2135	2126
SEA		
DJF	2169	1947
MAM	2225	1995
JJA	2222	1990
SON	2128	1909

Table A1.2. Nighttime precipitation frequency distributions in the SEP during the season with maximum drizzle occurrence (SON).

Year	Frequency				Total
	0.7 - 0.1	0.1 - 0.2	0.2 - 0.3	> 0.3	
2002	162031	323775	151958	40292	678057
2003	129510	371838	97852	43458	642657
2004	126920	331258	202323	47487	707988
2005	137281	311687	182465	62740	694174
2006	158290	303053	181602	27917	670862
2007	155412	271395	176421	110515	713744
2008	150807	297873	189085	66482	704247
2009	148217	293556	190524	56697	688993
2010	135554	301902	162895	128071	728422
				Average:	692127
				Std. dev:	25726
				Range:	85764.4

Table A1.3. Daytime precipitation frequency distributions in the SEP during the season with maximum drizzle occurrence (SON).

Year	Frequency				Total
	0.7 - 0.1	0.1 - 0.2	0.2 - 0.3	> 0.3	
2002	49789	5468	0	0	55258
2003	58999	6907	288	288	66482
2004	71374	8922	288	0	80584
2005	121452	19283	288	0	141022
2006	94974	10649	288	0	105910
2007	118574	21873	0	0	140446
2008	86916	13814	288	288	101306
2009	86628	12663	0	0	99291
2010	109364	11800	576	0	121739
				Average:	101338
				Std. dev:	30238
				Range:	85764

Table A1.4. Nighttime precipitation frequency distributions in the NEP during the season with maximum drizzle occurrence (JJA).

Year	Frequency				Total
	0.7 - 0.1	0.1 - 0.2	0.2 - 0.3	> 0.3	
2002	247796	234557	6619	0	488972
2003	267942	334424	13814	0	616180
2004	196855	414432	18419	0	629706
2005	191675	387667	15829	0	595170
2006	250674	412705	2878	0	666257
2007	235708	385364	7483	0	628555
2008	223908	221606	2015	0	447529
2009	162031	472280	119437	0	753748
2010	212684	512284	11800	0	736768
				Average:	618098
				Std. dev:	100836
				Range:	306219

Table A1.5. Daytime precipitation frequency distributions in the NEP during the season with maximum drizzle occurrence (JJA).

Year	Frequency				Total
	0.7 - 0.1	0.1 - 0.2	0.2 - 0.3	> 0.3	
2002	46048	5468	0	0	51516
2003	41443	5756	576	288	48063
2004	66194	4893	0	0	71087
2005	42307	4605	0	288	47199
2006	37990	2590	0	0	40580
2007	34248	1439	0	0	35687
2008	24751	1151	0	288	26190
2009	96701	8922	0	0	105623
2010	58423	2590	288	288	61589
				Average:	54170
				Std. dev:	23427
				Range:	79433

Table A1.6. Nighttime precipitation frequency distributions in the SEA during the season with maximum drizzle occurrence (SON).

Year	Frequency				Total
	0.7 - 0.1	0.1 - 0.2	0.2 - 0.3	> 0.3	
2002	251825	326653	4893	576	583946
2003	295858	421627	4605	576	722666
2004	283195	403496	21585	0	708276
2005	269669	337302	35112	576	642657
2006	236859	427383	70511	576	735329
2007	295858	322336	33097	0	651291
2008	217001	429398	29643	0	676042
2009	240889	355433	32809	288	629419
2010	226211	401193	23887	0	651291
				Average:	666769
				Std. dev:	48668
				Range:	151383

Table A1.7. Daytime precipitation frequency distributions in the SEA during the season with maximum drizzle occurrence (SON).

Year	Frequency				Total
	0.7 - 0.1	0.1 - 0.2	0.2 - 0.3	> 0.3	
2002	19858	0	0	0	19858
2003	49789	4893	0	0	54682
2004	34536	5180	0	0	39716
2005	59575	2590	0	0	62165
2006	105623	9497	0	0	115120
2007	47487	1439	0	0	48926
2008	35399	2302	0	0	37702
2009	32234	0	0	0	32234
2010	62740	5180	0	0	67921
				Average:	53147
				Std. dev:	27670
				Range:	95262

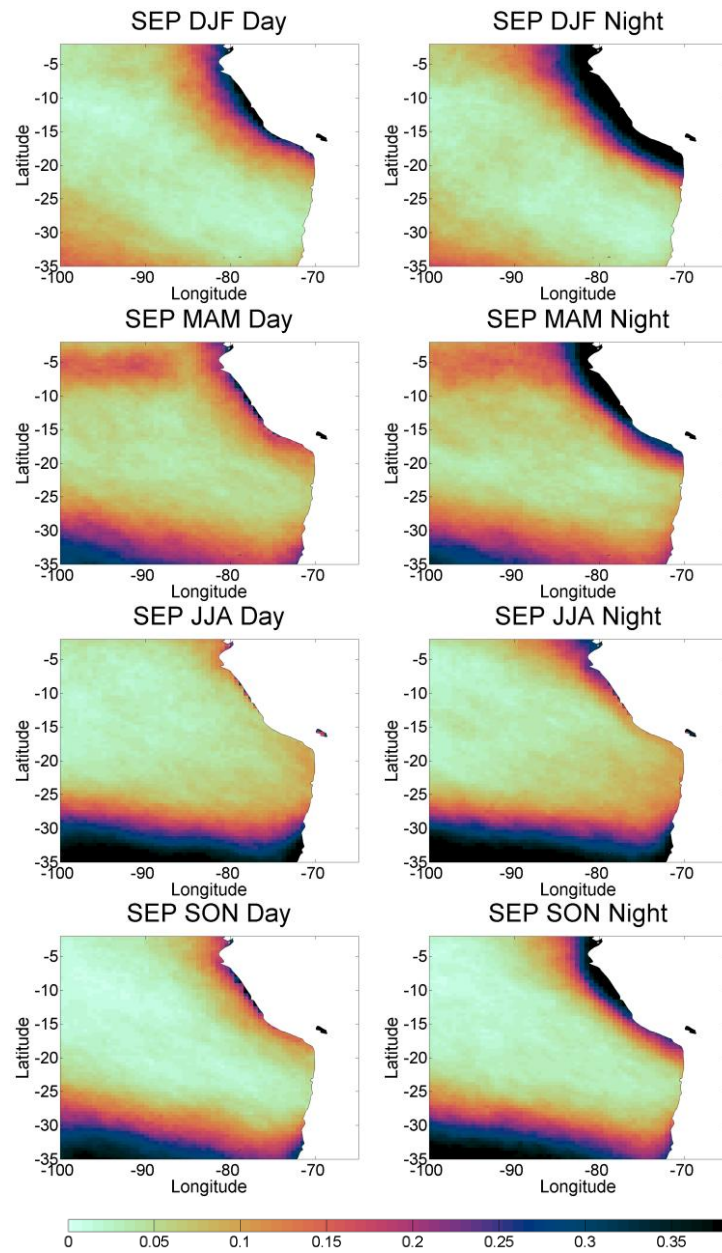


Figure A1.1. Distributions of ice-phase cloud frequency (% of pixels < 273 K, from MODIS cloud top temperature product) in the Southeast Pacific by season and time during the AMSR-E operational period from 2002-2011. The frequencies are normalized by sample size.

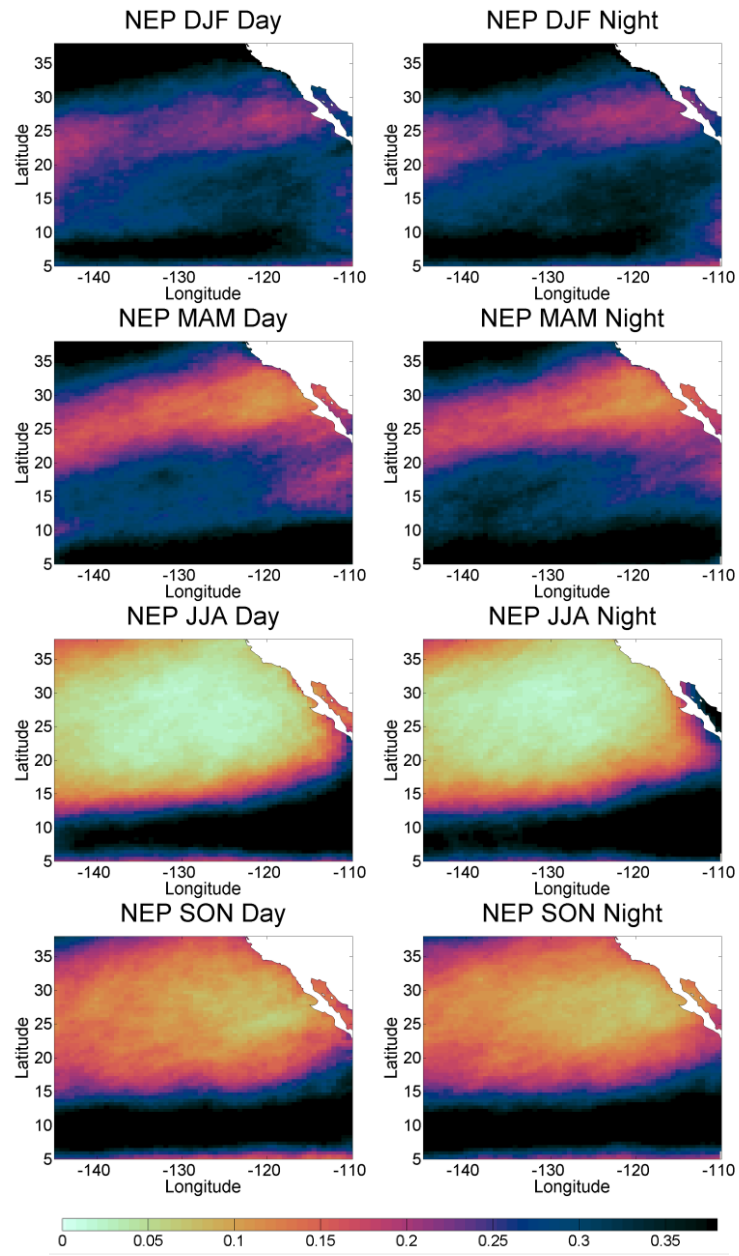


Figure A1.2. As in Figure A1.1 but in the Northeast Pacific.

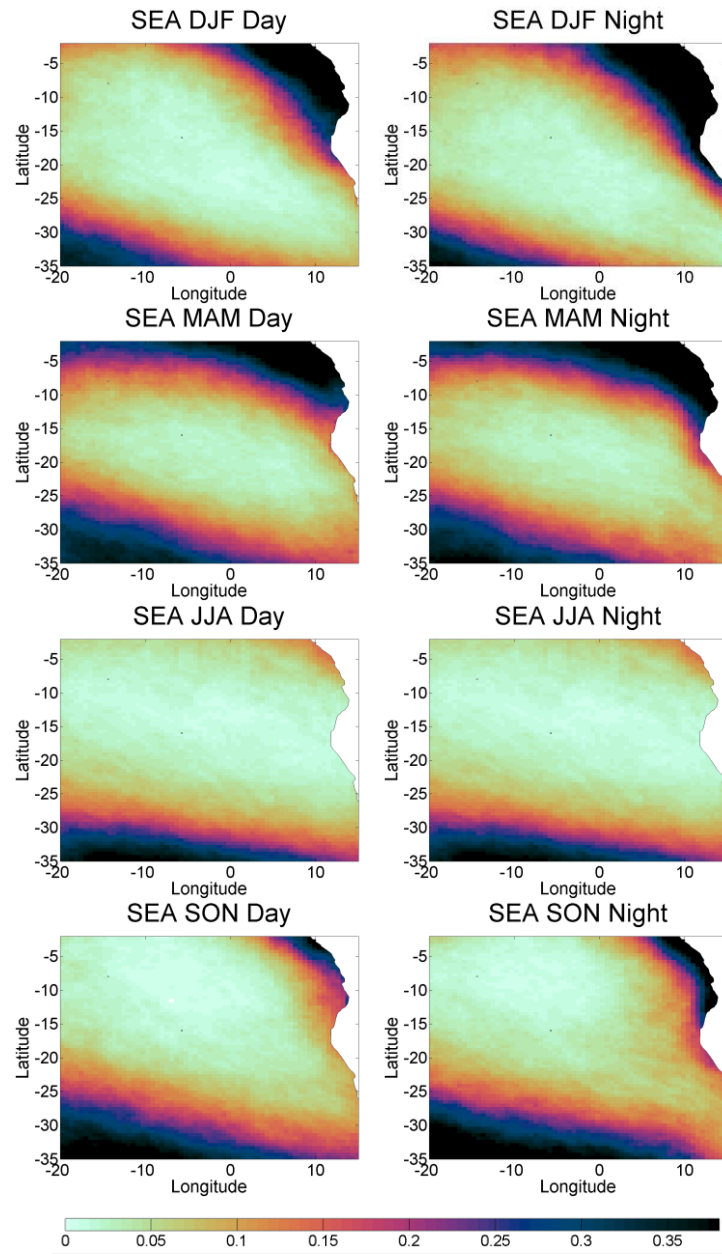


Figure A1.3. As in Figure A1.1 but in the Southeast Atlantic.

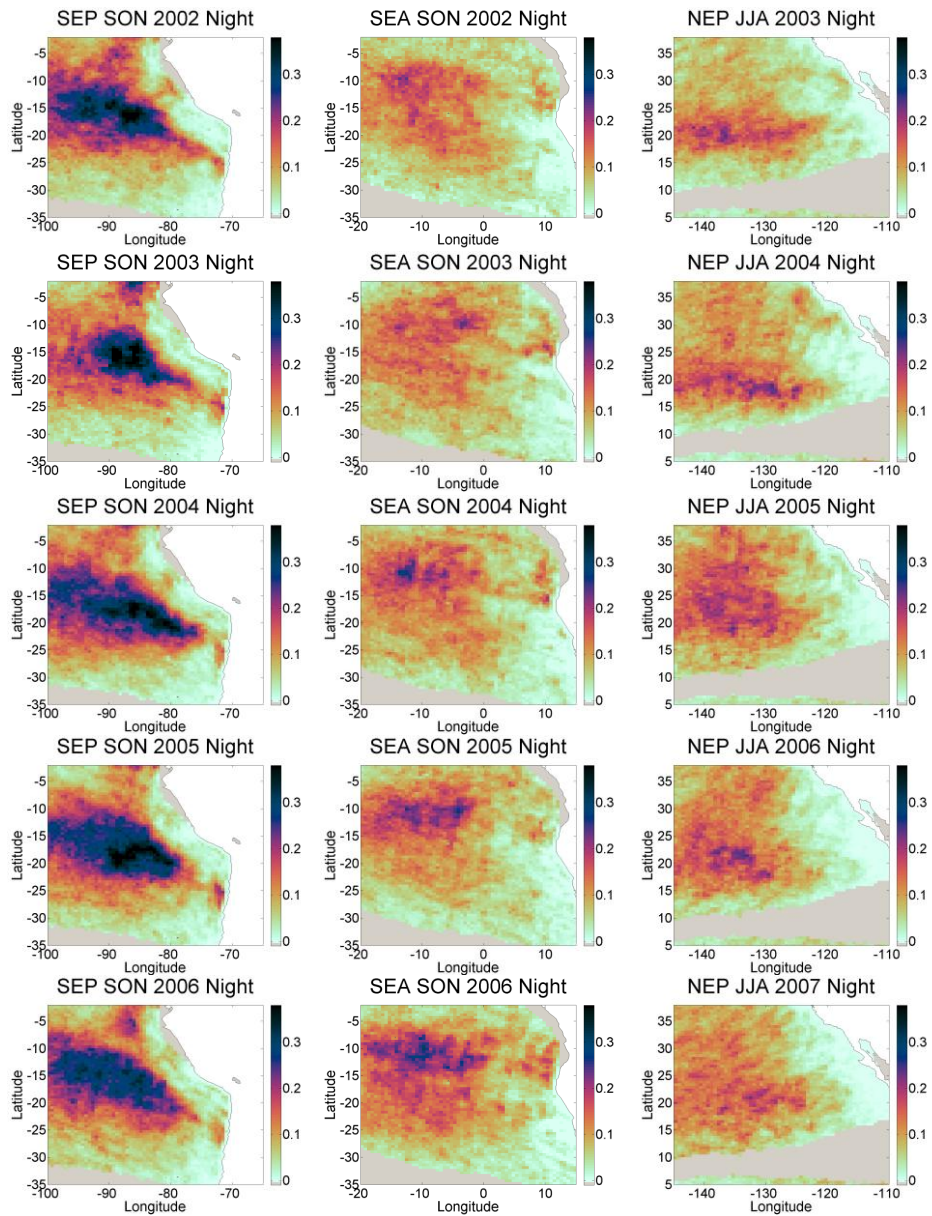


Figure A1.4. Nighttime drizzle frequency by year (2002-2006 SON; 2003-2007 JJA) for the season when precipitation maxima occur. Please note that the dataset does not include JJA 2002.

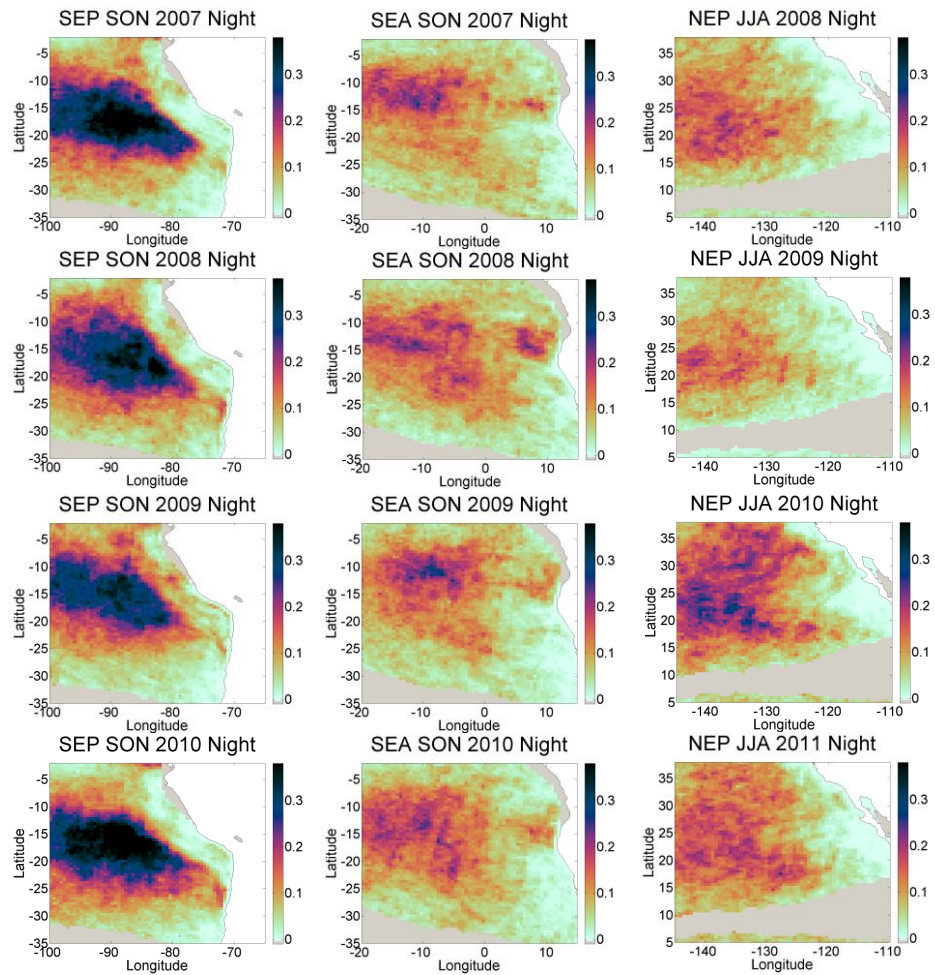


Figure A1.5. Nighttime drizzle frequency by year (2007-2010 SON; 2008-2011 JJA) for the season when precipitation maxima occur. Please note that the dataset does not include SON 2011.

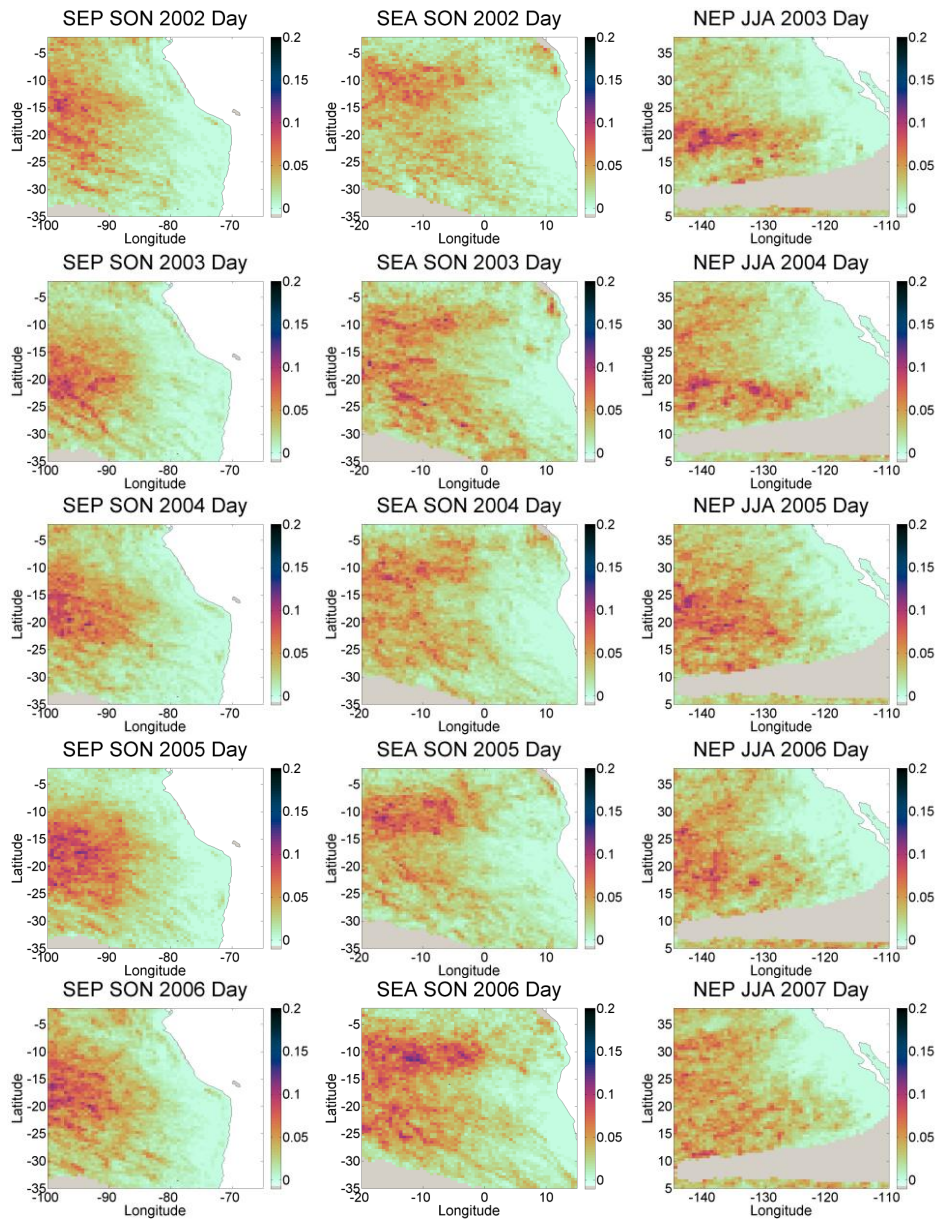


Figure A1.6. Daytime drizzle frequency by year (2002-2006 SON; 2003-2007 JJA) for the season when precipitation maxima occur. Please note that the dataset does not include JJA 2002.

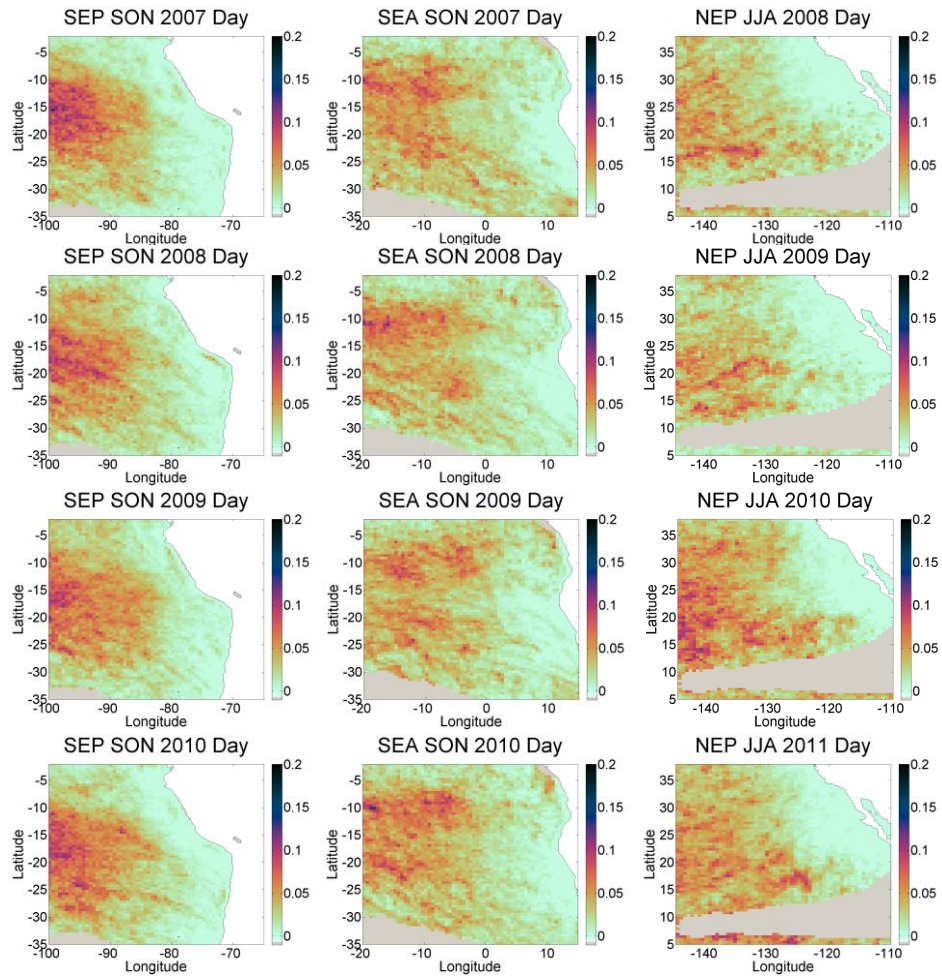


Figure A1.7. Daytime drizzle frequency by year (2007-2010 SON; 2008-2011 JJA) for the season when precipitation maxima occur. Please note that the dataset does not include SON 2011.